ChemElectroChem

Accepted Article

Title: Electrooxidation of Alcohols on Mixed Copper-Cobalt Hydroxycarbonates in Alkaline Solution

Authors: Michael Braun, Gereon Behrendt, Moritz L. Krebs, Patricia Dimitri, Piyush Kumar, Ignacio Sanjuán, Steffen Cychy, Ann Cathrin Brix, Dulce M. Morales, Jennifer Hörlöck, Bernd Hartke, Martin Muhler, Wolfgang Schuhmann, Malte Behrens, and Corina Andronescu

RESEARCH ARTICLE

Electrooxidation of Alcohols on Mixed Copper-Cobalt Hydroxycarbonates in Alkaline Solution

Michael Braun,[a]# Gereon Behrendt,[b]# Moritz L. Krebs,[c] Patricia Dimitri,[b] Piyush Kumar,[a,d] Ignacio Sanjuán,[a] Steffen Cychy,[e] Ann Cathrin Brix,[f] Dulce M. Morales,[g] Jennifer Hörlöck,[h] Bernd Hartke,[h] Martin Muhler,[e] Wolfgang Schuhmann,[f] Malte Behrens,*[b,c] Corina Andronescu*[a]

[a] M. Braun, P. Kumar, Dr. I. Sanjuán, Prof. C. Andronescu
     Chemical Technology III
     Faculty of Chemistry and CENIDE, Center for Nanointegration
     University of Duisburg-Essen
     Carl-Benz-Straße 199, 47057 Duisburg (Germany)
     E-mail: corina.andronescu@uni-due.de
[b] G. Behrendt, P. Dimitri, Prof. M. Behrens
     Institute of Inorganic Chemistry
     University of Duisburg-Essen
     Universitätsstr. 7, 45141 Essen (Germany)
[c] M. L. Krebs, Prof. M. Behrens
     Institute of Inorganic Chemistry
     Christian-Albrecht University of Kiel
     Max-Eyth-Str. 2, 24118 Kiel (Germany)
     E-mail: mbehrens@ac.uni-kiel.de
[d] P. Kumar
     Indian Institute of Science Education and Research (IISER)
     Dr. Homi Bhabha Road
     Pune 411008 (India)

[e] Dr. S. Cychy, Prof. M. Muhler
     Laboratory of Industrial Chemistry
     Faculty of Chemistry and Biochemistry; Ruhr University Bochum
     Universitätsstr. 150, 44801 Bochum (Germany)
[f] A. C. Brix, Prof. W. Schuhmann
     Analytical Chemistry, Center for Electrochemical Sciences (CES)
     Faculty of Chemistry and Biochemistry; Ruhr University Bochum
     Universitätsstr. 150, 44801 Bochum (Germany)
[g] Dr. D. M. Morales
     Nachwuchsgruppe „Gestaltung des
     Sauerstoffentwicklungsmechanismus"
     Helmholtz-Zentrum Berlin für Materialien and Energie GmbH
     Hahn-Meitner-Platz 1, 14109 Berlin (Germany)
[h] J. Hörlöck, Prof. B. Hartke
     Theoretical Chemistry
     Christian-Albrecht University of Kiel
     Max-Eyth-Str. 2, 24118 Kiel (Germany)

# These authors have contributed equally.

Supporting information for this article is given via a link at the end of the document.

Abstract: Mixed Cu-Co hydroxycarbonates of the type $(Cu_{1-x}Co_x)_2CO_3(OH)_2$ have been synthesized over the whole range of Cu-Co substitution ($0 \leq x \leq 1$) by co-precipitation and their electrocatalytic activity in the oxidation reactions of ethanol (EOR), ethylene glycol (EGOR) and glycerol (GOR) in alkaline environment was evaluated to retrieve composition–activity correlations. Generally, cobalt incorporation led to higher activities for the alcohol oxidation (AOR) compared to the Cu-only material and the results are compared with the competing oxygen evolution reaction (OER). On the Cu-Co hydroxycarbonates, the electrooxidation of vicinal alcohols such as glycerol and ethylene glycol requires lower overpotentials than EOR and OER. Cu leaching from the hydroxycarbonate structure was observed in the presence of vicinal alcohols. The impact of chemical and electrochemical leaching of copper from the catalysts has been studied. The chemically leached catalyst was found to show increased AOR activity compared to other hydroxycarbonates, enabling the formation of larger amounts of formic acid during GOR measured in a circular flow cell electrolyzer. The results highlight that Cu-Co hydroxycarbonates can be used as precursors to generate electrocatalytically active materials from Cu-Co hydroxycarbonates for the AOR in alkaline solution.

Introduction

Electrochemical water splitting using green energy could be the ecofriendly alternative to generate hydrogen as a valuable industrial chemical, potential energy carrier and fuel.[1,2] In parallel to the electrochemical hydrogen evolution reaction (HER) at the cathode, oxygen is formed at the anode in the oxygen evolution reaction (OER). While in HER, two protons coupled to two electrons are transferred, OER requires the transfer of four electrons and protons, thus being a sluggish reaction showing slow kinetics and higher overpotentials which decrease the overall energy efficiency of water electrolysis.[3,4] Therefore, substituting water oxidation by other reactions requiring lower overpotentials while producing H_2 at the cathode, described as a "chemical-assisted hydrogen evolution reaction", could make electrocatalytic hydrogen production economically feasible.[5,6] Additionally, by replacing O_2 formation, possibilities open up also at the anode for the generation of value-added chemicals, which can be paired with H_2 formation at the cathode via water splitting.[7,8]

As such, the electrochemical oxidation of organic compounds, for example, alcohols,[9,10] amines,[11] urea,[12] and hydrazine[13] has gained increasing interest in the last years. It has been shown that alcohols such as ethanol,[14,15] ethylene glycol,[16,17] and glycerol[18–20] can be converted in alkaline electrolyte at overpotentials that are typically lower than those required for water oxidation. Glycerol is especially interesting since it is readily and inexpensively obtained as a biomass-derived byproduct in biodiesel production. Furthermore, glycerol is referred to as a platform chemical since its oxidation products can have applications in many fields, such as pharmaceutics, personal care products, or polymers.[21–23] For example, the C1-product formic acid (or its conjugated base formate) is used as a metal surface treatment agent, rubber additive or as the fuel in fuel cells.[24,25]

Highly active electrocatalysts for the electrochemical alcohol oxidation reaction (AOR) are usually found among the platinum

RESEARCH ARTICLE

group metals. Yet their scarcity, high price, sensitivity to CO-poisoning, and the low current densities often recorded make them unsuitable for future industrial applications, where H_2 production needs to be conducted at a current density in the A cm^{-2} range. Therefore, earth-abundant and low-priced 3d transition metal-based electrocatalysts have been studied for AOR, with nickel being one of the most common metals used in this regard, offering not only high current densities and stability but also high selectivity in alkaline conditions.[10,26–28]

Copper or cobalt are also among the materials used for the electrochemical oxidation of ethanol,[29–32] ethylene glycol,[33,34] and glycerol.[34–37] Moreover, the combination of both Cu and Co in bimetallic systems has been shown to be electrocatalytically advantageous for the electrochemical glycerol oxidation reaction (GOR).[38–40] Zhu et al. synthesized a CuCo-MOF/polyaniline composite, which revealed higher electrocatalytic activity for GOR than the corresponding monometallic Cu-/Co-MOF or the pure CuCo-MOF without polyaniline in 0.5 M KOH and 0.5 M glycerol.[38] El-Nagar et al. prepared a catalyst series of metal-doped-Cu$_2$O/Cu by using a dynamic hydrogen bubble template technique, tested for GOR in 2 mM glycerol and 0.1 M KOH solution. On Co-doped Cu$_2$O/Cu dendrites, higher current densities were recorded than on the corresponding Ni- and Fe-doped catalysts, which could not be entirely explained by the increased surface area of the doped material.[40] Furthermore, Han et al. demonstrated that the nanostructured spinel of CuCo$_2$O$_4$ can outperform the MCo$_2$O$_4$ analogues with M = Mn, Fe, Co, Ni, Zn in terms of activity in 0.1 M glycerol and 1.0 M KOH and showed that CuCo$_2$O$_4$ was most selective for the production of formic acid at 1.3 V vs. RHE.[39]

Cu-based hydroxycarbonates derived from malachite Cu$_2$CO$_3$(OH)$_2$ are an interesting material class to study the effect of the catalyst composition in more detail as they can incorporate other bi-valent 3d transition metal cations in the hydroxycarbonate lattice such as Co^{2+}. This substitution approach is well-established for layered double hydroxide electrocatalysts,[41–45] but seldomly applied to other hydroxycarbonates such as substituted malachites. Their substitution ability has made them well-known precursor materials in heterogeneous catalysts used for the synthesis of Cu/ZnO catalysts in the industrial methanol synthesis from syngas. They are typically synthesized as mixed Cu, Zn, (Al) hydroxycarbonates by co-precipitation.[46,47] So far, these hydroxycarbonates have been explored in electrocatalysis only in their pure Co or Ni- and Mn-substituted form for OER, HER and oxygen reduction reaction.[48–53] To the best of our knowledge, there has not been a comprehensive study yet on the systematic variation of different transition metal cations in malachite-type catalysts for the AOR.

In this work, a series of mixed Cu and Co hydroxycarbonates, synthesized by co-precipitation and subsequent hydrothermal treatment, are explored for the OER and the electrochemical oxidations of ethanol (EOR), ethylene glycol (EGOR) and glycerol (GOR) in alkaline electrolyte by cyclic voltammetry. In addition, competition of AOR with OER studied by differential electrochemical mass spectrometry (DEMS), and the chemical stability of the Cu:Co 80:20 catalyst in KOH electrolytes containing different alcohol is presented. Moreover, leaching of Cu is investigated using rotating-disk electrode (RDE) experiments and flow-cell electrolyzers, as a step to further increase the AOR conversion on the hydroxycarbonates.

Results and Discussion

Synthesis and characterization of Cu-Co hydroxycabonates

Mixed metal hydroxycarbonates (Cu$_{1-x}$Co$_x$)$_2$CO$_3$(OH)$_2$ have been synthesized over the whole range of Cu:Co ratios based on a procedure used to prepare zincian malachite described elsewhere.[54] Samples are labelled with the nominal molar metal content, e.g. "Cu:Co 80:20" for 80 at.% Cu and 20 at.% Co, referring to a (Cu$_{0.8}$Co$_{0.2}$)$_2$CO$_3$(OH)$_2$.

Elemental analysis evaluated by atomic absorption spectroscopy (AAS) and elemental analysis of C, H, N and S (CHNS) showed that both metals were successfully incorporated into the obtained hydroxycarbonate, and the H:C ratio is well in agreement with the nominal 2:1 stoichiometry in (Cu,Co)$_2$CO$_3$(OH)$_2$ (Figure 1, Figure S1). Moreover, we can distinguish three regions in the composition space: Cu-rich samples are likely to be found in the malachite structure Cu$_2$CO$_3$(OH)$_2$; this is valid here for samples with a Co substitution of up to 20%. For nearly equimolar Cu:Co ratios around 50:50, the kolwezite structure is expected, which is isostructural to the Cu-Zn mineral rosasite (Cu,Zn)$_2$CO$_3$(OH)$_2$.[55–58] This can be attributed to the region of ca. 35–50% Co, and, in fact, for the transition sample Cu:Co 70:30 a relatively large deviation from the expected ratio was found and reproduced for a second batch. This indicates that the substitution of Co into the malachite structure has found an end here, and that this sample rather forms a group with the samples of similar experimental metal ratios (Cu:Co 60:40 and 50:50). On the Co-rich end of the series, a pure Co hydroxycarbonate exists[59] (no equivalent mineral known), that, presumably, can be substituted with Cu up to 40% according to the linear trend we found for the incorporated metal ratios. However, the small deviation of these samples from the nominal values might point to an asymptotic behavior and a substitution limit somewhere below 60% Co, in the region where we thus find the kolwezite or rosasite structure type instead. In any case, all crystal structures of malachite, kolwezite, and cobalt hydroxycarbonate are closely related and show the same composition of the anionic sub-lattice according to M_2CO$_3$(OH)$_2$.
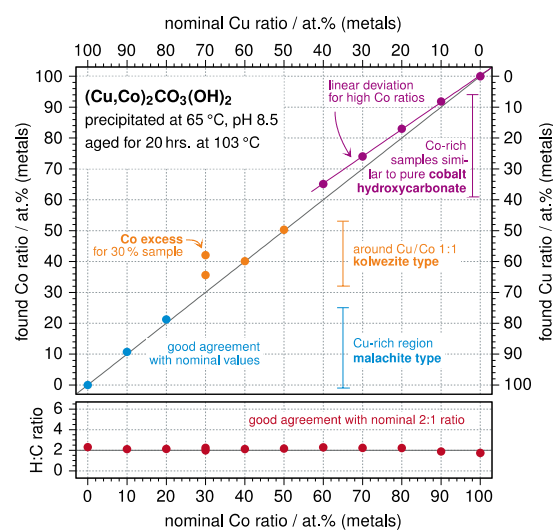

Figure 1. Elemental analysis of the synthesized Cu-Co hydroxycarbonates. The H:C ratio is in good agreement with the nominal 2:1 stoichiometry in (Cu,Co)$_2$CO$_3$(OH)$_2$; for the metal ratios we see deviations from the expected values for the sample with nominally 30% Co and for Co-rich samples and therefore distinguish three regions in the composition space.

RESEARCH ARTICLE

The distinction of these three groups in the composition space (malachite type, kolwezite/rosasite type, cobalt hydroxycarbonate type) is supported by powder diffraction data (Figure 2): The patterns for the samples Cu 100, Cu:Co 90:10 and 80:20 match well with the reference pattern for malachite. Here we know from the literature on Zn-substituted "zincian malachite" that the substitution of Cu^{2+} by other ions decreases the degree of Jahn-Teller distortion in the respective MO_6 octahedra, which leads to a lattice contraction in the crystallographic c direction and therefore to a shift of Bragg reflections with significant share of c to larger 2θ angles.[46] This behavior is also found in our Cu-Co substitution series, at least for the very first step from pure copper malachite to $(Cu,Co)_2CO_3(OH)_2$ with 10% Co (Figure 2). For the "kolwezite region" around Cu:Co 50:50 we use the isostructural rosasite as reference and see a good agreement with the samples Cu:Co 70:30, 60:40, and 50:50, spanning the range of ca. 35–50% Co. For a pure cobalt hydroxycarbonate, we have been supplied with a reference pattern by Girgsdies et al.[59] and high similarities in the patterns of the Co-rich samples Cu:Co 40:60, 30:70, 20:80, 10:90 and Co 100 can be found.
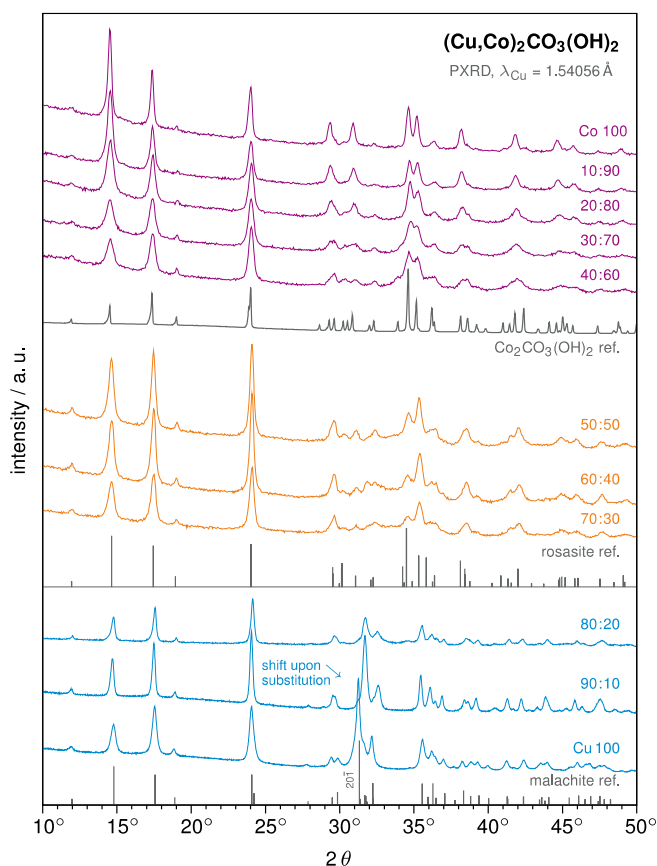
between malachite and rosasite (which we again use as the reference for the isostructural kolwezite) are found for the CO_3^{2-} out-of-plane bending vibration v_2 and in the fingerprint region between 400 and 850 cm^{-1}. Here, we are able to assign the Cu-rich samples Cu 100, Cu:Co 90:10 and 80:20 very well to the reference pattern of malachite and the samples 70:30, 60:40 and 50:50 match the rosasite pattern except for slight differences between $(Cu,Zn)_2CO_3(OH)_2$ and $(Cu,Co)_2CO_3(OH)_2$ that have to be taken into consideration. Regarding the pure cobalt hydroxycarbonate, we take our own sample as the reference for the upper limit of the substitution series and see again a good agreement with the patterns of Cu:Co 10:90 and 20:80; however, in case of the samples Cu:Co 30:70 and 40:60 there is also a certain similarity to the rosasite pattern of the "kolwezite region" samples, hinting at how one pattern could evolve from the other. This might also be valid for the respective crystal structures. Whereas the step from rosasite/kolwezite to malachite is very clear (as can be seen by the different patterns in IR, powder X-Ray diffraction (PXRD), and also in the broad gap we found in elemental analysis, see Figure 1), the transition from kolwezite to the pure cobalt hydroxycarbonate might be relatively smooth (cf. Table S1 in the Supporting Information) — in fact, some authors assign cobalt hydroxycarbonate to the rosasite structure type, which would imply unlimited substitutability between the "kolwezite region" and the Co-rich samples.[56,57]

Figure 2. Powder diffraction (PXRD) patterns of the synthesized Cu-Co hydroxycarbonates. Cu-rich samples match the malachite pattern and also show the characteristic shift of the $20\bar{1}$ reflection to higher 2θ angles upon substitution of Cu. The samples Cu:Co 70:30, 60:40, and 50:50 can be attributed to the rosasite structure type (kolwezite); Co-rich samples ≥ 60% show very similar patterns to the pure cobalt hydroxycarbonate. Reference patterns from ICSD (nos. 100150 and 109166) and [59] given with square root intensity to enlarge small signals.
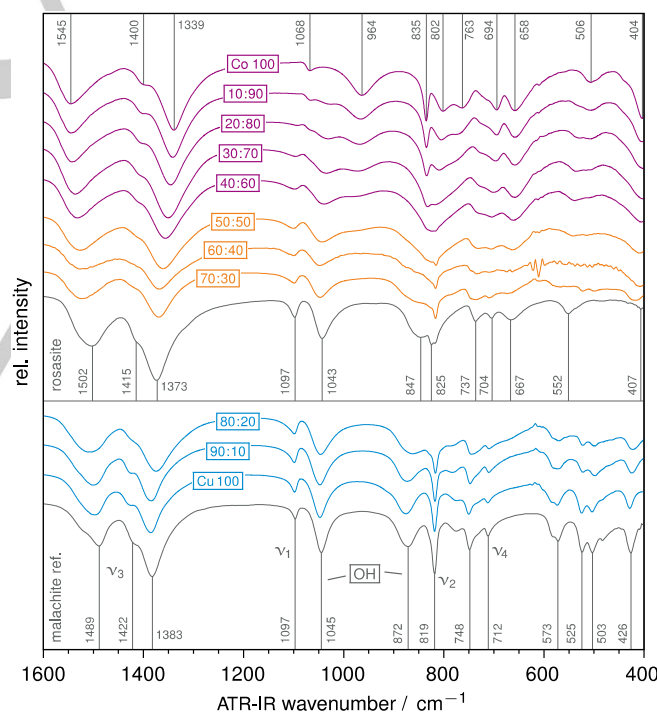

Figure 3. Infrared (IR) spectra of the synthesized Cu-Co hydroxycarbonates. Similar to the findings in PXRD, Cu-rich samples match the malachite reference pattern, the samples in the "kolwezite region" match the isostructural rosasite, and the Co-rich samples are similar among each other. Here, the transition from the "kolwezite region" to the Co-rich zone is less distinct, and the samples Cu:Co 40:60 and 30:70 might also be attributed to rosasite/kolwezite. Reference patterns from RRUFF database (nos. R050508 and R050294) with CO_3^{2-} vibrations (v_{1-4}) and OH out-of-plane bending labelled.[60]

Infrared spectroscopy (IR) of the sample series supports our classification in the Cu-rich zone, the "kolwezite region", and the Co-rich part of the composition space. The main differences

Scanning electron microscopy (SEM) revealed that different morphologies are formed depending on the cobalt content of the sample: Cu-rich samples (Cu:Co 90:10, 80:20) show a fluffy

3

RESEARCH ARTICLE

morphology, larger magnification reveals very regular bodies with a square cross section — cubes and cuboids — that might be part of longer rods, as we know malachite (and Zn-substituted zincian malachite) to form needles.[46] In contrast, Co-rich samples are composed of platelets stacked onto or wedged into one another. Especially the comparison of the Cu-rich sample Cu:Co 80:20 with Cu:Co 70:30 from the "kolwezite region" now shows a surprisingly clear transition between both samples. Other, "dandelion-like" morphologies for high Co contents are shown in the Supporting Information (Figure S2).
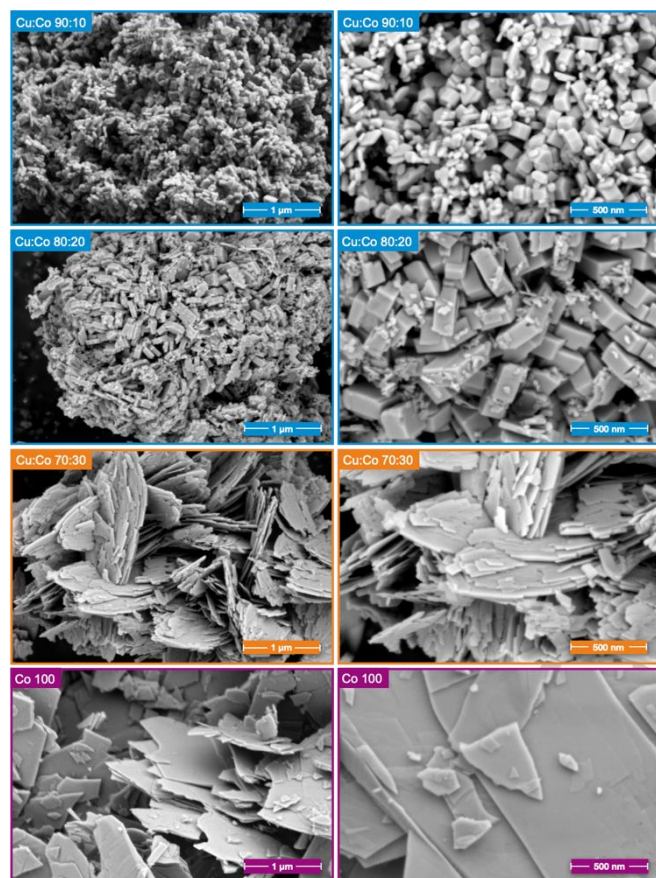

Figure 4. Scanning electron microscopy images of selected Cu-Co hydroxycarbonate samples at two levels of magnification. Cu-rich samples exhibit a fluffy morphology consisting of cubes and cuboids; whereas medium and Co-rich samples are composed of platelets — here, the transition from the Cu-rich sample Cu:Co 80:20 to the 70:30 sample ("kolwezite region") is really clear.

Electrocatalytic activity of the Co-Cu hydroxycarbonates

The electrocatalytic activity of the mixed Cu-Co hydroxycarbonate series was evaluated after drop casting the respective catalyst on a polished glassy carbon electrode and recording three consecutive cyclic voltammograms (CV) using RDE in Ar-saturated 1 M KOH as electrolyte. The first recorded CV is used to evaluate the activity of the pristine hydroxycarbonates, while the second and the third ones provide a brief assessment of changes in the electrocatalytic activity induced by possible structural modification usually reported at relatively high anodic potentials. Initially, we evaluated the OER activity, which will be used as a reference to assess the electrocatalytic activity of the Cu/Co-based materials to later compare with the investigated

alcohol electrooxidation reactions. The first CV scans for selected materials from the series are shown in Figure 5a, while the CVs from all hydroxycarbonates are presented in Figure S3. Figure 5b shows an overview of the current density recorded at 1.60 V vs. RHE in all three CVs for all catalysts. The results indicate that the OER activity of the hydroxycarbonates is influenced by their Cu:Co ratio. While the pure Cu hydroxycarbonate shows negligible electrocatalytic activity for the OER, the addition of Co boosts the OER activity. A volcano-type correlation can be observed with increasing Co concentration, the highest activity being recorded for the sample Cu:Co 40:60 in the transition region between kolwezite and cobalt hydroxycarbonate when analyzing the first scan of the CVs. A further increase in the Co content with respect to Cu over 60% leads to a decrease in the electrocatalytic OER activity. However, by performing three CVs in the OER region, changes in the electrocatalytic OER activity were observed especially for the Co-rich samples for which an increased electrocatalytic was recorded. This can be attributed to an increased CoOOH-formation at higher potentials, whose oxidation was reported to be important for the OER activity on Ni- and Mn-substituted Co hydroxycarbonate catalysts.[48]
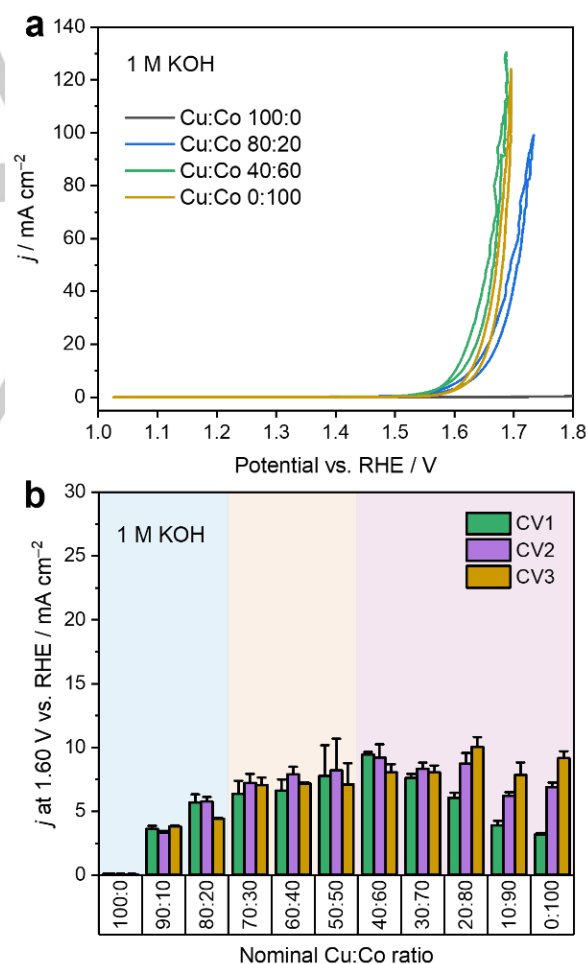

Figure 5. Activity of the mixed Cu-Co hydroxycarbonate series towards OER. **a)** First CV scan recorded on hydroxycarbonates with different Cu:Co ratios. For clarity, not all Cu:Co ratios are shown (cf. Figure S5). **b)** Current densities recorded at 1.60 V vs. RHE in the anodic scan of three consecutive CVs, plotted as a function of the corresponding nominal Cu:Co ratio. The CVs were recorded at a scan rate of 5 mV s^{-1} and electrode rotation of 1600 rpm in Ar-saturated 1 M KOH.

RESEARCH ARTICLE

The electrocatalytic activity of the Cu-Co hydroxycarbonates in the electrooxidation of alcohols was evaluated using a similar protocol as for the OER, with the difference that 0.1 M of the specific alcohol (ethanol, ethylene glycol, or glycerol) was added to the 1 M KOH solution. The recorded CVs (Figure 7a, c and e, cf. Figure S4–S6) show specific shapes depending on the alcohol present in the electrolyte, further exemplified for the Cu:Co 80:20 catalyst (Figure 6a). The corresponding graphs showing the recorded currents in the presence and absence of the alcohols for the whole Cu-Co hydroxycarbonate series are shown in Figure S7. On Cu:Co 80:20, the currents recorded in the presence of ethanol are slightly different from those recorded in KOH only. An increase in the current can be observed at a potential slightly higher than 1.4 V vs. RHE, which remains overall constant until a sudden increase in the current occurs at potentials at which OER is observed when using only KOH electrolyte. Overall, in the OER region, slightly lower currents are recorded in the presence of ethanol compared with the KOH solution only. A drastic change is observed when glycerol is added to the KOH solution. In this case, several features can be observed in the first CV scan. At ~1.4 V vs. RHE, an increase in the oxidation current is observed, followed by an inflection point at ~1.6 V vs. RHE (dotted line in Figure 6a), a maximum at 1.67 V vs. RHE, and a slight decrease in the current at higher potentials. Significantly lower currents are recorded during the cathodic scan compared with the anodic scan. In the presence of ethylene glycol, lower currents than in glycerol-

containing KOH are initially recorded, which sharp increase at ~1.6 V vs. RHE. Also, a considerably smaller cathodic than anodic current is recorded in this case. The magnitude of the hysteresis observed between anodic and cathodic scan decreases with the number of OH groups present in the alcohol: glycerol > ethylene glycol > ethanol ~ KOH solution, which may indicate that changes in the catalyst structure or on its surface take place.

Overall, we see that AOR occurs on the Cu-Co hydroxycarbonates in the same potential window as the OER, therefore the currents recorded in the CV is a convolution of both processes. To evaluate the OER contribution to the registered current, we used DEMS, thus determining the potential window in which OER occurs when alcohols are added to the electrolyte, using Cu:Co 80:20 as catalyst (Figure 6b, c and d). Irrespective of the alcohol, at potentials below 1.50 V vs. RHE, no O_2 was detected, indicating that the currents observed at ~1.4 V vs. RHE are only from the AOR or surface reactions such as catalyst oxidation. In all three cases, we see a significant increase in the O_2 amount (converted in Figure 6 into oxygen partial current densities) at potentials higher than 1.55 V vs. RHE for ethanol or 1.60 V vs. RHE for glycerol and ethylene glycol. Additionally, OER seems to be suppressed in the presence of vicinal alcohols at higher potentials. The overpotential at which OER becomes significant is higher.
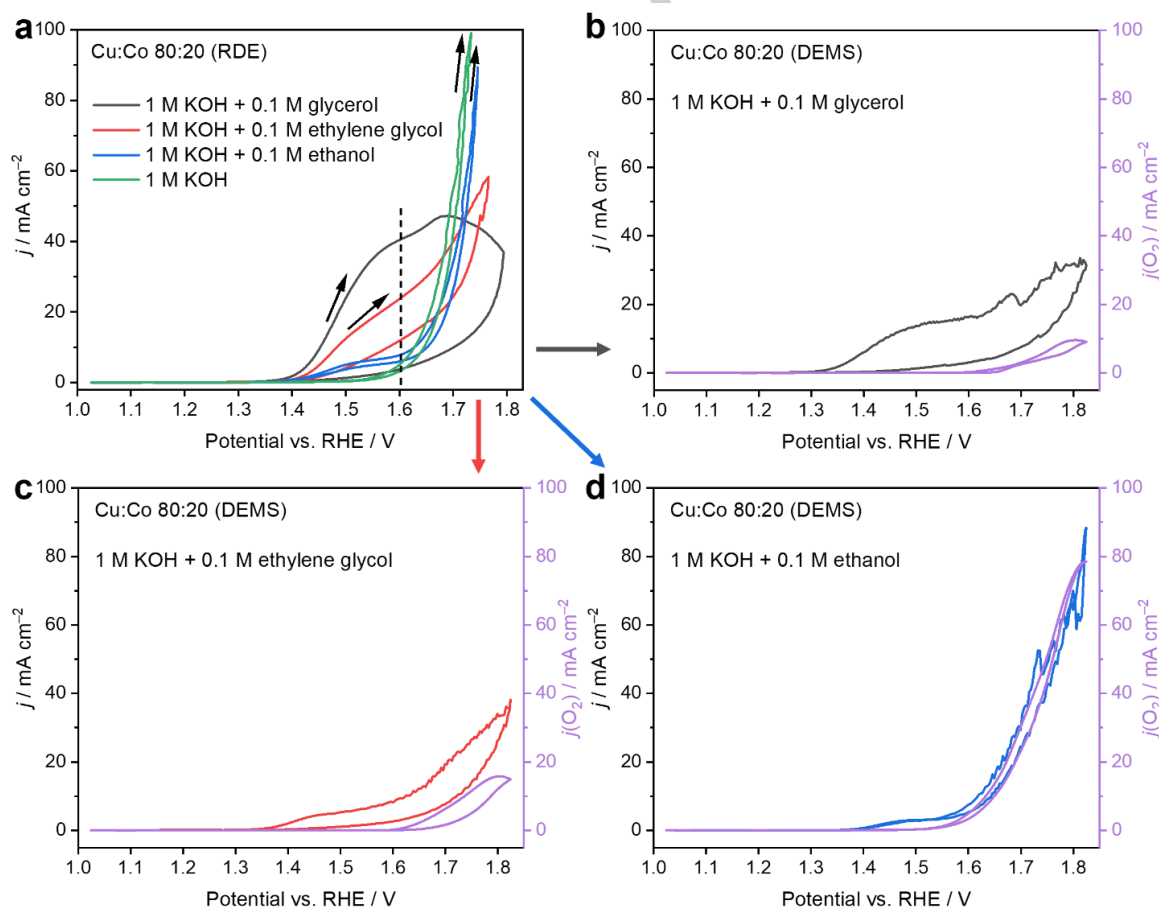

Figure 6. RDE and DEMS measurements using Cu:Co 80:20 for the OER and AOR. **a)** First CV recorded by RDE at a scan rate of 5 mV s^{-1} and electrode rotation of 1600 rpm in Ar-saturated 1 M KOH or 1 M KOH + 0.1 M of alcohol; potentials are corrected for the iR-drop. **b, c, d)** CVs recorded in DEMS (grey - b, red - c or blue - d) overlapped with the derived current densities (violet) based on the MS signal m/z = 32 (in Torr) recorded in Ar-saturated 1 M KOH + **b)** 0.1 M glycerol, **c)**

RESEARCH ARTICLE

0.1 M ethylene glycol, **d)** 0.1 M ethanol at a scan rate of 0.5 mV s^{-1} and a flow rate of 10 uL min^{-1}. The recorded DEMS signals at m/z = 32 (in Torr) were converted to currents (in mA) using a calibration coefficient obtained with a reported active and stable OER catalyst that provided 100% faradaic efficiency for OER in 1 M KOH. The potentials recorded in the DEMS measurements are not corrected for the iR-drop.

In the presence of ethanol, the detected O$_2$ almost perfectly matches the recorded currents, while for ethylene glycol and glycerol, we see that less than half of the recorded currents can be attributed to OER. This observation highlights that part of the OER active sites on the catalyst surface also becomes active for the glycerol and ethylene glycol electrooxidation at a high enough anodic potential or they are just blocked by these molecules or their reaction products.
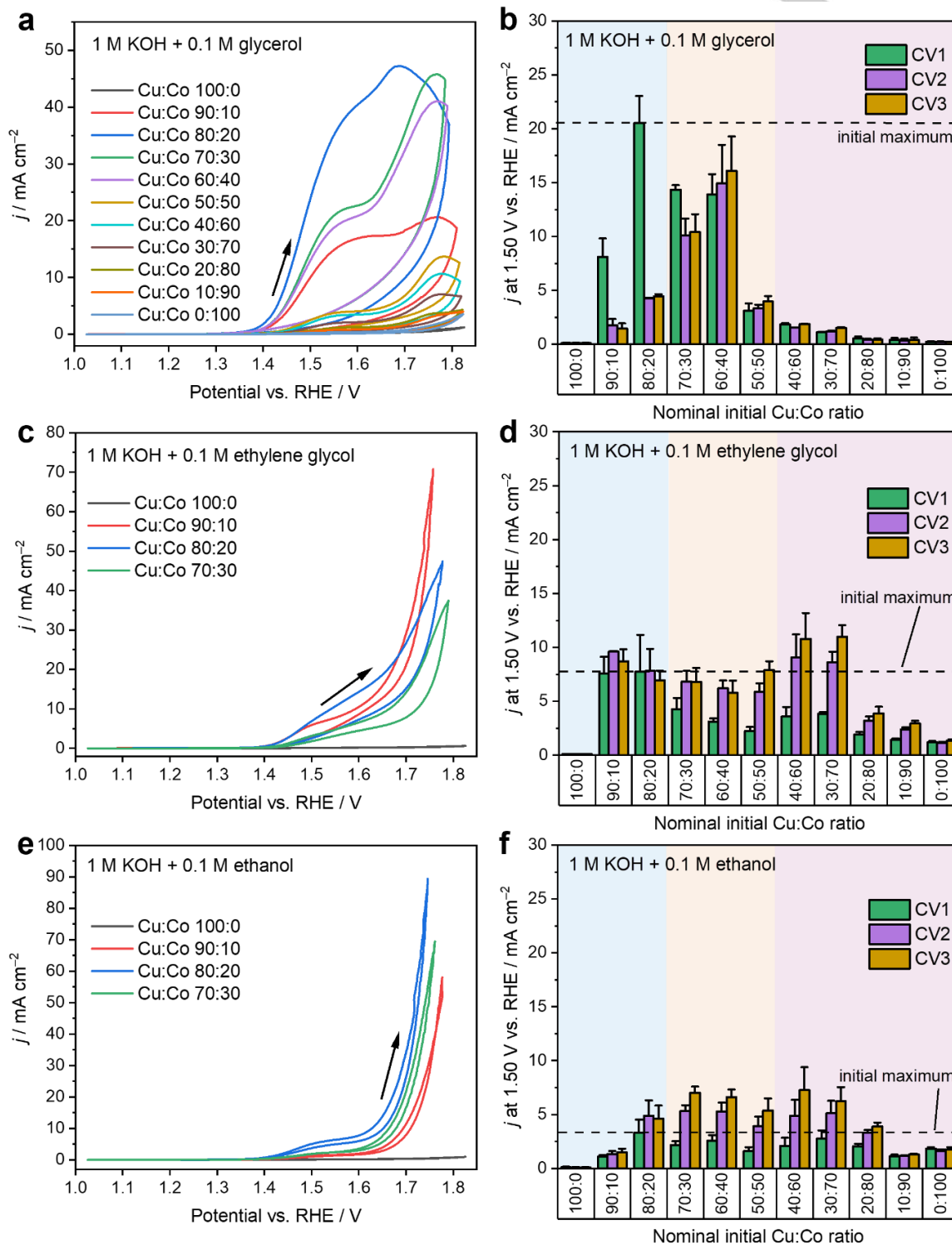
RESEARCH ARTICLE

Figure 7. AOR on the Cu-Co hydroxycarbonate series evaluated by RDE voltammetry at a scan rate of 5 mV s^{-1}and electrode rotation of 1600 rpm in Ar-saturated 1 M KOH + 0.1 M of **a,b)** glycerol, **c,d)** ethylene glycol and **e,f)** ethanol. **a,c,e)** Example of first CVs obtained in the presence of selected Cu-Co hydroxycarbonates. For clarity, not all Cu:Co ratios are shown in c and e (cf. Figure S4–S6). Current densities recorded in the anodic scan of three consecutive CVs at 1.50 V vs. RHE for the **b)** GOR, **d)** EGOR and **f)** EOR as a function of the corresponding nominal initial Cu:Co ratios.

To evaluate the influence of the catalyst structure and composition on the AOR, we compared the currents recorded at 1.50 V vs. RHE (Figure 7b, d and f) where negligible OER currents are recorded in the RDE measurements (Figure 5a). Thus we expect no significant OER contribution during AOR, which was confirmed by DEMS for the Cu:Co 80:20. As for OER the pure Cu hydroxycarbonate shows no electrocatalytic activity towards AOR while the pure Co hydroxycarbonate is inactive for the GOR and shows a minimum activity for the EOR and the EGOR. The substitution of Cu with Co leads to a significant increase in the recorded current densities with an initial maximum catalytic activity evaluated from the first CV reached for the Co-richest malachite sample, Cu:Co 80:20, in all three alcohols (also cf. Figure S4–S6). While in the case of EOR and EGOR the Cu:Co 80:20 activity is not significantly higher than that of the other Cu:Co catalysts, for GOR the Cu:Co 80:20 shows comparatively high activity with ~25% higher current densities than the Cu:Co 70:30 and 60:40.

By further decreasing the Cu content below 80 at.% and thus entering the kolwezite region, a decrease in the AOR activity is observed, most steadily during GOR, while for EGOR and EOR a second activity maximum is recorded for the Cu:Co ratio of 30:70. Independent of the alcohol present in the KOH solution, the bimetallic catalysts showed increased activity for AOR compared with the monometallic Cu or Co analogues. The hydroxycarbonate with a Cu:Co ratio of 80:20 appeared to be particularly active for AOR, especially for GOR. Additionally, higher Cu contents seem to be advantageous for the vicinal alcohol oxidation in terms of current density at 1.50 V vs. RHE, while for ethanol no significant impact of the composition is noticeable since the recorded currents are below 5 mA cm^{-2}. Nevertheless, the observed differences in activity may result from a combined effect between the different Cu:Co ratios, the structural modifications in the hydroxycarbonate and the higher reactivity of the triol or diol compared to a mono-alcohol resulting from a higher number of OH groups or lower pKa values.[61] Furthermore, it should be emphasized that the activity differences observed may be also related to the likely different electrochemically active surface areas of the various catalysts, although the specific surface areas are very similar in a range of 11.5 to 23.5 cm^2 g^{-1} (Figure S8).

When comparing the currents recorded at 1.50 V vs. RHE in the first CV scan with the ones recorded in the third CV scan significant changes in the electrocatalytic AOR activity of all Cu-Co hydroxycarbonates are observed. For example, the activity of catalysts with nominal initial Cu contents of 70–90 at.% (with respect to the total metal content of Cu and Co) is reduced after the first cycle during GOR, whereas catalysts with a Cu content lower than 70 at.% show a slightly increased activity. After three CVs the Cu:Co 60:40 located in the kolwezite region has become the most active catalyst for GOR. In the case of EGOR and EOR, the catalysts with 20–70 at.% Cu show an enhanced activity after three CVs with the highest current density in the third CV recorded for the Cu:Co 30:70 and 40:60 catalysts situated in the transition regions between kolwezite and the cobalt hydroxycarbonate structure.

The observed changes in the recorded currents indicate changes in the structure and/or composition of the electrocatalysts, which seem to be pronounced in GOR for Cu:Co 80:20, where the initially active catalyst loses its activity. In contrast, the Cu:Co 60:40 catalyst shows a slight increase in the activity, which could indicate parallel activation and deactivation processes, with the activation process predominating (Figure 7b). Possible activation and deactivation processes will also be further addressed at a later phase of the study. In addition to structural and compositional changes within the catalyst, the effects of surface modification by adsorbates cannot be excluded. For example, deactivation processes that relate to strongly adsorbed intermediates during e.g. GOR have not only been reported for noble metals such as Pt,[62] but also for non-noble metal-based catalysts like LaNiO$_3$.[35] Besides, the upper limit potential chosen in the electrocatalytic measurements can influence the current response and stability of the catalyst over the course of the consecutive CVs. When the Cu:Co 80:20 catalyst was exposed to lower upper limit potentials during the CV scans, where OER currents were not observed in DEMS measurements (Figure 6), the strong hysteresis was not obtained and even a small activation was found at an upper potential limit of 1.52 V vs. RHE (Figure S9), indicating probably that a more oxidative environment of a parallel starting OER may speed up the deactivation process. Further studies were thus conducted using the Cu:Co 80:20 catalyst to understand the reasons for the deactivation.

In an initial step, we checked for the chemical stability of the Cu:Co 80:20 catalyst in the KOH electrolyte in the absence of the applied potential by immersing a catalyst sample in 1 M KOH. While no visible coloring of the electrolyte occurs in this case, we observed an immediate change in the solution color from colorless to blue, once we immersed the catalyst in a solution containing 1 M KOH and 0.1 M glycerol, which is typical for Cu polyalcoholate complexes. For the pure Cu hydroxycarbonate, we observed a total dissolution of the catalyst in the mixture of KOH and glycerol, while for the pure Co hydroxycarbonate, no color change could be observed (Figure S10). We further investigated the metal content of several hydroxycarbonates after 4 h immersion in 1 M KOH and 0.1 M glycerol by inductively coupled plasma optical emission spectrometry (ICP-OES) shown in Figure 8a. The Cu loss determined from ICP-OES was higher for the hydroxycarbonates with higher initial Cu ratio, almost 20 at.% for the Cu:Co 80:20 catalyst, whereas Cu:Co 50:50 and 40:60 showed a Cu loss of only ~1%, indicating that Cu leaching occurs mainly in the Cu-rich hydroxycarbonates when glycerol is present in the alkaline environment. It is known that Cu^{2+} can form complexes with vicinal polyalcohols such as glycerol, saccharose or even cellulose in an alkaline solution.[63–66] This fact was previously used, for example, in the electrodeposition of Cu^{2+} from a cyanide-free alkaline glycerol solution or in the production of rayon by dissolving cellulose in Schweizer's reagent (a tetraamine copper(II) hydroxide solution).[63,64] Gadd[65] found that vicinal alcohols can act as bidentate ligands in alkaline solution for complexation of Cu^{2+} and suggested that deprotonation of the OH groups at higher pH is required for the formation of the respective complexes. It was also found that the copper-to-alcohol stoichiometry of the formed compounds was close to 1:1. Furthermore, it was shown that the relative complex stability of Cu^{2+} with glycerol, ethylene glycol and propane-1,2-diol, homogeneously

RESEARCH ARTICLE

dissolved in KOH solution, increase in the following order: ethylene glycol < propane-1,2-diol < glycerol. Monohydric alcohols would not show this complex formation.[65] These results can explain our experimental observation and we would expect that glycerol chemically leaches Cu more effectively than ethylene glycol at a similar pH, whereas ethanol does not lead to a chemical leaching.
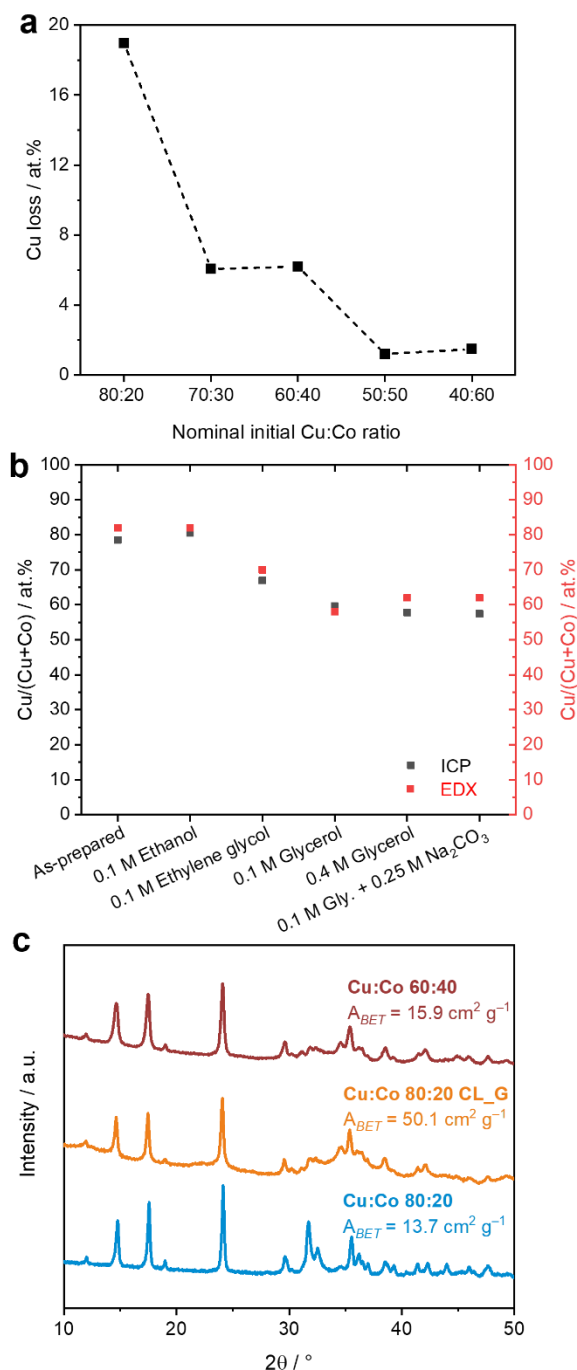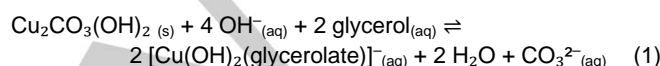

Figure 8. Investigation of chemical leaching (CL) of Cu from selected hydroxycarbonates. **a)** Relative Cu loss after chemical leaching of selected hydroxycarbonates with different Cu:Co ratios in 0.1 M glycerol and 1 M KOH for 4 h measured by ICP-OES. **b)** Relative Cu content after immersing the Cu:Co 80:20 catalyst in 1 M KOH solutions with different alcohols for 4 h obtained by ICP-OES and EDX measurements. **c)** PXRD patterns and corresponding BET-surface area (A$_{BET}$) of as-prepared Cu:Co 80:20, Cu:Co 60:40 and Cu:Co 80:20 immersed for 4 h in 0.1 M glycerol and 1 M KOH (labelled Cu:Co 80:20 CL_G).

To confirm this, the Cu and Co content of the Cu:Co 80:20 catalyst immersed for 4 h in 1 M KOH solution containing 0.1 M glycerol, 0.1 M ethylene glycol or 0.1 M ethanol, was evaluated and the Cu content in at.% is presented in Figure 8b. After immersing the catalyst in the alcohol-containing KOH solution, we observed that the highest decrease in the relative Cu content occurs for the sample immersed in glycerol followed by ethylene glycol, while ethanol does not show any leaching effect in comparison to the as-prepared catalyst. Upon increasing the glycerol concentration to 0.4 M or using a mixture of 0.1 glycerol and 0.25 M Na$_2$CO$_3$ in 1 M KOH, the relative Cu content was still ~60 at.%. Since the Cu content is not different compared to the usage of 0.1 M glycerol in 1 M KOH, this may imply that an equilibrium stage is reached within the duration of the experiment that cannot be shifted towards a higher degree of Cu leaching by using a higher concentration of glycerol or towards a lower degree of Cu leaching by addition of carbonate ions according to eq. 1 assuming mono-deprotonated glycerol and a monoanionic complex.[65]

$$Cu_2CO_3(OH)_{2\ (s)} + 4\ OH^-_{(aq)} + 2\ glycerol_{(aq)} \rightleftharpoons$$
$$2\ [Cu(OH)_2(glycerolate)]^-_{(aq)} + 2\ H_2O + CO_3^{2-}_{(aq)} \quad (1)$$

In the following paragraphs we will use "Cu:Co 80:20 CL_G" to refer to the Cu:Co 80:20 catalyst immersed for 4 h in 1 M KOH containing 0.1 M glycerol. This chemical leaching shifts the composition of the hydroxycarbonate from the malachite into the kolwezite region and indeed the PXRD analysis of Cu:Co 80:20 CL_G indicates that the Cu:Cu 80:20 catalyst (malachite type structure) changes during the 4 h immersion in the glycerol-containing KOH solution to a structure more similar to the Cu:Co 60:40 which we attributed to the kolwezite structure (Figure 8c). In addition to the structural change, also the specific surface area was found to increase as a result of Cu leaching. Nitrogen physisorption following the method of Brunauer, Emmett, and Teller (BET) (Figure S8),[67] showed a more than threefold increase in the surface area likely as a result of enhanced porosity and roughness due to the Cu loss from the solid (Figure 8c).

To evaluate how the Cu leaching influences the electrocatalytic activity of the Cu:Co 80:20 electrocatalyst, we performed prolonged electrolysis at 1.43 V vs. RHE in 1 M KOH containing 0.1 M glycerol using a RDE setup. Before and after 2, 4 and 21 h electrolysis, we evaluated the electrochemical surface area (ECSA) based on the double layer capacitance by immersing the catalyst-modified electrode in KOH solution only (Figure 9, Figure S12). In the first minutes, we observed an increase in the recorded current up to a maximum followed by a continuous decrease over the initial 2 h electrolysis. While the increasing current may be due to an increased surface area as a consequence of the leaching process, it could also be an activation process caused by the transition of the catalyst modification to an intermediate highly active state, such as the change from malachite to the kolwezite structure for instance. The ECSA recorded after 2 h of electrolysis shows a more than 8-fold higher value than the freshly deposited catalyst, which is in good qualitative agreement with the results obtained by physisorption on the chemically leached sample and further supports the idea of pore formation during the leaching process. The relatively high value implies that the deactivation of the catalyst film may be the reason for the observed decay in the recorded current. Surprisingly, after reintroducing the electrode that was before exposed to 1 M KOH during the ECSA determination, in the glycerol containing electrolyte, we observe a regaining of the initial activity followed by a continuous decay over the next 2 h of
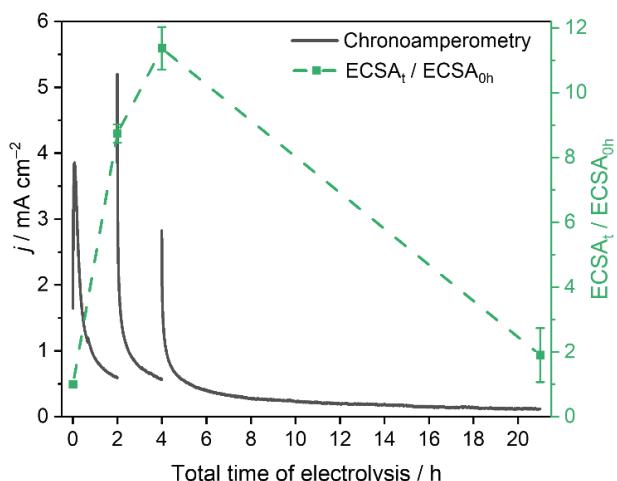
RESEARCH ARTICLE

Figure 9. Chronoamperometric measurements of the Cu:Co 80:20 catalyst in 0.1 M glycerol and 1 M KOH on RDE at a potential of 1.43 V vs. RHE and a rotation speed of 1600 rpm (black line). The electrochemical surface area was determined at 0, 2, 4 and 21 h in 1 M KOH by measurements of the electrochemical double-layer capacitance via cyclic voltammetry. The obtained $ECSA_t$ (with t = 0, 2,4 and 21 h) is given in relation to the initial ECSA recorded at 0 h (green dashed line).

electrolysis, despite the calculated ECSA after a total electrolysis time of 4 h shows an even higher value than after 2 h. Busó-Rogero et al. found during EOR on Pt single crystals in alkaline media that the initial activity of Pt(111), which decreased during several CVs due to blocking species resulting from the polymerization of acetaldehyde on the electrode surface, could be restored by a subsequent rinsing step with water before electrochemical cycling in KOH electrolyte and reintroducing the electrode in the previous ethanol-containing KOH solution.[68] Since these results, as well as the measurement procedure, are similar to the observed activation and reactivation processes depicted in Figure 9 and aldehydes can also be formed during GOR, a blocking of the active sites by polymerization of the reactive intermediates on the electrode surface, which can be removed in neutral pH, cannot be excluded and may provide an explanation for the observations in Figure 9. This suggests that the properties of the working catalyst are highly dynamic and adjust in a fast manner to changes in the experimental conditions.

A similar current profile is observed when we reintroduced the catalyst-modified electrode for the third time in the electrolyte with a continuously slow current decay during the 17 h electrolysis. After a total electrolysis time of 21 h, the measured ECSA significantly decreased, reaching almost the value obtained for the ECSA of the freshly catalyst-coated electrode. The decrease of the ECSA observed between 4 and 21 h electrolysis may be due to a significant loss of catalyst particles or be caused by deposition of organic films which can be formed by the previously mentioned polymerization of e.g. aldehydes formed as intermediate species during GOR. Moreover, the recorded currents during the measurement may have an effect on the local pH close to the electrode surface, which could in turn affect the concentration of specific products at the interface and thus also the stability of the catalyst, as it was suggested in literature.[69,70]

To understand the reason behind the observed decrease in ECSA and the deactivation of the catalyst, we used SEM and X-ray photoelectron spectroscopy (XPS) to study the catalyst film morphology and the metal composition on the electrode surface. For this purpose, a glassy carbon plate was coated with the Cu:Co 80:20 catalyst and was subsequently partially immersed in the

electrolyte for 4 h. After this time, part of the electrode was retracted from the electrolyte and the electrolysis was conducted for the still immersed part for another 17 h at 1.43 V vs. RHE (Figure S12). Based on the SEM images, we observed that significant changes in the catalyst structure occur after 4 h and a total of 21 h electrolysis (Figure 10a). The as-prepared catalyst film shows visible catalyst agglomerates that are no longer present after electrolysis, indicating a dissolution or partial detachment of the catalyst film. XPS analysis conducted on the three distinct areas of the electrode allowed the calculation of the relative Cu content (reported to the total metal content of Cu and Co) on the electrode surface. We observed a significant decrease in the Cu content from an initial ~73 at.% to ~15 at.% and below 10 at.% after 4 h and 21 h of electrolysis, respectively (Figure 10b). Besides the Cu:Co ratio modification, changes in the Co oxidation state are also noticed. While the dominant oxidation state in the as-prepared catalyst on the electrode is Co^{2+} in a $CoO/Co(OH)_2$ species, which is demonstrated by the main peak at ~781 eV and a satellite peak present at ~785 eV being in good agreement with spectra of $Co_2(CO_3)(OH)_2$,[49,53] the presence of a new satellite peak at 791 eV indicates the formation of a Co_3O_4 species after electrolysis (Figure 10c).[71] In the following, we will use "EL_G_4h" to indicate electrochemically induced leaching, which refers to the sample after electrolysis performed in 0.1 M glycerol and 1 M KOH for 4 h at 1.43 V vs. RHE.

To identify possible changes in the bulk and crystalline structure during the 4 h electrolysis (Cu:Co 80:20 EL_G_4h), multiple electrodes modified with the Cu:Co 80:20 catalyst were run to collect a sufficient amount for the structural characterization by PXRD and EDX analysis. Using EDX, the relative Cu content with respect to the total metal content was calculated to be 16 at.% in the Cu:Co 80:20 EL_G_4h sample in agreement with the above-mentioned XPS results, which yielded a relative Cu content of 15%. The agreement between the two techniques indicates that electrochemical leaching affects not only the surface but also the bulk of the catalyst. Additionally, and compared to the Cu:Co 80:20 CL_G, which still had ~60 at.% of Cu (EDX) after 4 h, the leaching occurring during the electrolysis goes beyond the previously determined equilibrium limit and does not stop at the kolwezite region. The results of the Cu:Co ratios from leaching Cu:Co 80:20 either chemically or electrochemically and measured by the different techniques are summarized in Table S2. Considering glycerol's degree of dissociation[72] in 1 M KOH to be approx. 40% using a pKa value of 14.15[61] for the first deprotonation step and an H^+ concentration of 10^{-14} mol L^{-1}, we assume that the positive potential at the anode can hence act as an additional driving force attracting more negatively charged glycerolate ions from the electrolyte, which can then leach out more Cu from the catalyst than without an applied potential. Interestingly, the powder diffractogram shows that significant changes in the crystalline structure of Cu:Co 80:20 occur during 4 h electrolysis, different from the ones observed in Cu:Co 80:20 CL_G: New reflections at $2\theta = 36°$, $39°$, and $49°$ indicate the formation of CuO, whereas the former malachite or intermediate kolwezite structure has only small contributions at $2\theta = 17.5°$ and $24°$ (inset in Figure 10b). Co_3O_4 as suggested by the XPS results, was not found to be present in a crystalline form. We thus assume that the Cu:Co 80:20 malachite catalyst is subjected to structural modifications during electrocatalytic GOR, which include the intermediate change to the kolwezite structure that can be triggered already by chemical leaching but go strongly beyond this change under applied potential.
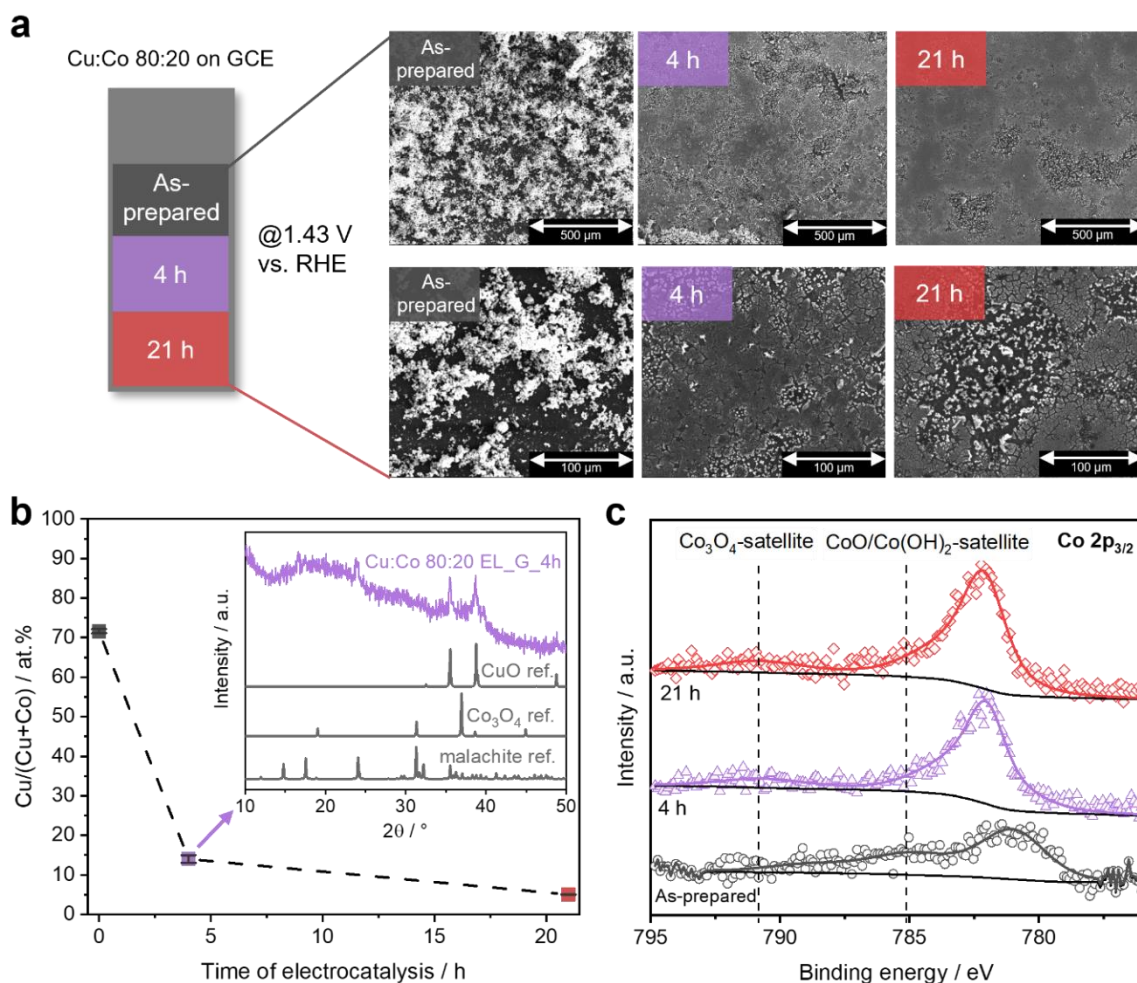
Figure 10. Investigation of the electrochemical leaching of Cu:Co 80:20. **a)** Scheme of the catalyst coated glassy carbon electrode (GCE) containing three areas: as-prepared - not in contact with the electrolyte; 4 h/21 h - in contact with the electrolyte at a potential of 1.43 V vs. RHE for 4 h and 21 h, respectively. SEM images of the respective parts of the GCE are depicted in the scheme at different magnifications. **b)** Relative Cu content with respect to the total metal content evaluated from peak areas of the XPS Cu $2p_{3/2}$ and Co $2p_{3/2}$ high-resolution spectra. Inset: PXRD patterns for the Cu:Co 80:20 after 4 h of electrolysis at 1.43 V vs. RHE in 1 M KOH and 0.1 M glycerol (violet). Reference patterns taken from ICSD (Nos. 100150 (malachite), 9362 (Co_3O_4) and 16025 (CuO)). The PXRD pattern of Cu:Co 80:20 EL_G_4h is different to the one obtained after chemical leaching for Cu:Co 80:20 CL_G as presented in Figure 8c. **c)** High-resolution XPS Co $2p_{3/2}$ spectra recorded on the three different regions of the catalyst coated electrode.

This results in a highly dynamic modified state of the initial catalyst, for which we observe interesting high activity not only in the first CV scan, but also transiently in chronoamperometric measurements after renewed immersion in the glycerol containing electrolyte. As we do not expect the crystalline CuO component of the catalyst to be solely responsible for this state, we focus in the following paragraph on the 85 at.% Co-containing fraction that formed as a residue of electrochemical Cu^{2+} leaching from the mixed hydroxycarbonate.

Computational study

In order to assess the reactivity of the (electro-)chemically leached sample for GOR, we performed Genetic Algorithms calculations on selected structures derived from pure or mixed Cu-Co hydroxycarbonates. Since the PXRD investigation has largely shown a loss of crystallinity, and the specific surface area and ECSA both suggest a nano-structuring effect of the leaching, we assume the as-prepared flat crystal surfaces (Figure 4) to transform into a rough and corrugated surface or possibly porous

aggregates on a length scale of a few atoms. Therefore, we employed finite-size clusters as models for such a leached and hence presumably highly corrugated surface.

Investigating globally optimized Cu-Co hydroxycarbonate clusters with a Cu:Co ratio of 80:20 shows that adsorption to Cu atoms is stronger than adsorption to Co atoms, both for protonated and mono-deprotonated glycerol. In such clusters, the coordination geometries around Cu or Co can be assumed to be optimal, except for the inevitable surface distortions imposed by the small cluster size. Although we made no attempt to simulate the actual leaching process, this observation may be seen as supporting the notion of preferential Cu leaching.

Further investigations were carried out both with pure cobalt hydroxycarbonate clusters and modified Cu-Co hydroxycarbonate clusters, in which Cu atoms were substituted by Co atoms. The former clusters were globally optimized as such and can be compared to the initial Cu:Co 80:20 sample and the pure Co hydroxycarbonate that is Cu-free as per synthesis, whereas the latter ones were globally optimized in their original Cu-Co form, followed by Cu-to-Co replacement and a local structure optimi-

RESEARCH ARTICLE

zation to represent the leached state. Although leaching of Cu does not equal substitution by Co, these distorted clusters are perceived as a model for the Cu-deficient hydroxycarbonate after leaching in which only Co is present in a former structure of the Cu-Co hydroxycarbonate.

Figure 11 shows examples of the lowest energy adsorption geometries of protonated and mono-deprotonated glycerol for all three types of investigated clusters. Possible adsorption geometries of glycerol are mono-coordinated, bi-coordinated as a bridge between two metal atoms, or as a bidentate ligand on one metal atom. As pointed out before, in the mixed clusters both protonated and mono-deprotonated glycerol prefer to adsorb on Cu atoms instead of Co atoms.
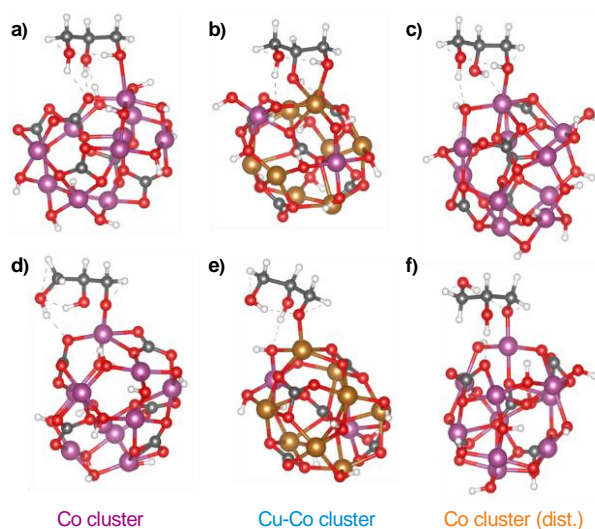

Co cluster   Cu-Co cluster   Co cluster (dist.)

Figure 11. Exemplary adsorption geometries of glycerol (a–c) and mono-deprotonated glycerol (d–f) on different Cu-Co hydroxycarbonate clusters. In **a,d)** globally optimized pure Co hydroxycarbonate cluster; **b,e)** mixed Cu-Co hydroxycarbonate cluster with a Cu:Co ratio of 80:20, also globally optimized; **c,f)** modified Co hydroxycarbonate cluster derived from b/e and locally optimized after Cu-to-Co replacement to yield a distorted Co-only cluster derived from the mixed state.
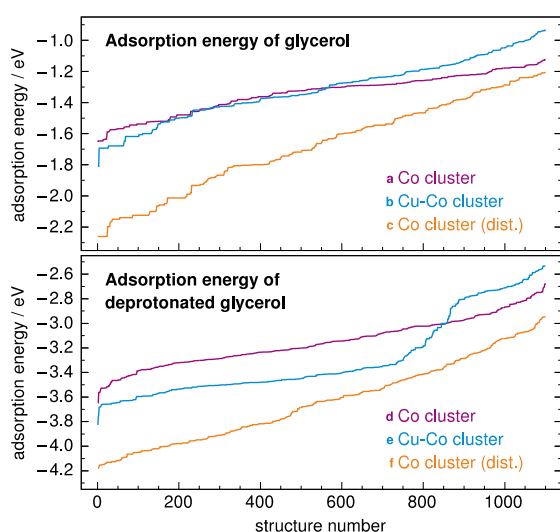

Figure 12. Adsorption energies of protonated (*top*) and mono-deprotonated glycerol (*bottom*) on different Cu-Co hydroxycarbonate clusters with the general composition $(Cu,Co)_2CO_3(OH)_2 \times 5$. (a–f) denote pure Co and mixed Cu-Co clusters as well as distorted Co cluster as depicted in Figure 11.

Glycerol often adsorbs bi-coordinated as bidentate ligand, whereas deprotonated glycerol prefers the mono-coordinated state on top of a Cu atom. In the globally optimized, pure Co clusters, glycerol, as well as mono-deprotonated glycerol, prefer the mono-coordinated state. In the case of the modified (distorted), Cu-to-Co replaced Co clusters, deprotonated glycerol usually is mono-coordinated. In contrast, glycerol as such seems to be mono-coordinated as often as bi-coordinated.

Adsorption energies of glycerol and mono-deprotonated glycerol are illustrated in Figure 12. In the Cu-Co substituted clusters, adsorption both by protonated and mono-deprotonated glycerol is much stronger on these distorted, Cu-deficient clusters than in the other cases. In such clusters, the coordination geometry around Co atoms cannot be as regular as in the globally optimized ones, naturally leading to a stronger interaction with an additional bonding partner. The observed adsorption energy difference — or in other words, the improved glycerol adsorption capability of the modified Co cluster — indicate that previously not accessible Co centers could be exposed by the removal of Cu atoms during leaching, which might lead to an increased activity of the catalyst. However, actual computational exploration of ensuing catalytical reaction steps will be subject of future work.

Electrocatalytic effects of chemical leaching of Cu:Co 80:20

Considering the computational findings on a potential activity increase in the GOR due to the chemical leaching, we evaluated the electrocatalytic activity of the Cu:Co 80:20 CL_G sample, which achieved the highest Cu leaching degree without the assistance of an external potential (Figure 8) for the electrooxidation of the three alcohols glycerol, ethylene glycol and ethanol. The results were compared to those recorded for the Cu:Co 80:20 and for the Cu:Co 0:100 catalysts representing the not yet Cu-deficient initial state and the by synthesis Co-enriched and thus undistorted state of the Co hydroxycarbonate. The electrocatalytic activity of Cu:Co 80:20 CL_G towards AOR using RDE voltammetric measurements was similarly investigated as formerly described, and the first and second CVs for the GOR are presented in Figure 13a (cf. Figure S13). It can be observed that the currents recorded in the first CV on the Cu:Co 80:20 CL_G during the GOR are lower than those recorded on the Cu:Co 80:20 catalyst and higher than obtained on the catalyst with a Cu:Co ratio of 0:100. As previously seen, in the second CV scan the currents on Cu:Co 80:20 drastically decrease in the anodic scan and Cu:Co 0:100 shows no significant change in activity while Cu:Co 80:20 CL_G also retains its initial activity. As a result, Cu:Co 80:20 CL_G becomes the most active GOR catalyst among the others reported in the present study. The stability of Cu:Co 80:20 CL_G strongly suggests that the changes of Cu:Co 80:20 between the different CVs is related to the occurrence of Cu leaching and can be suppressed by previous chemical leaching of the catalyst. This activity trend is also observable after three CV scans as shown in Fig. 13b, where the currents recorded on the respective catalysts at 1.50 V vs. RHE are presented. Among the compared samples, Cu:Co 80:20 CL_G is the most active catalyst for EOR and EGOR in all CVs (Figure 13c and d); and for GOR after the first CV scan.
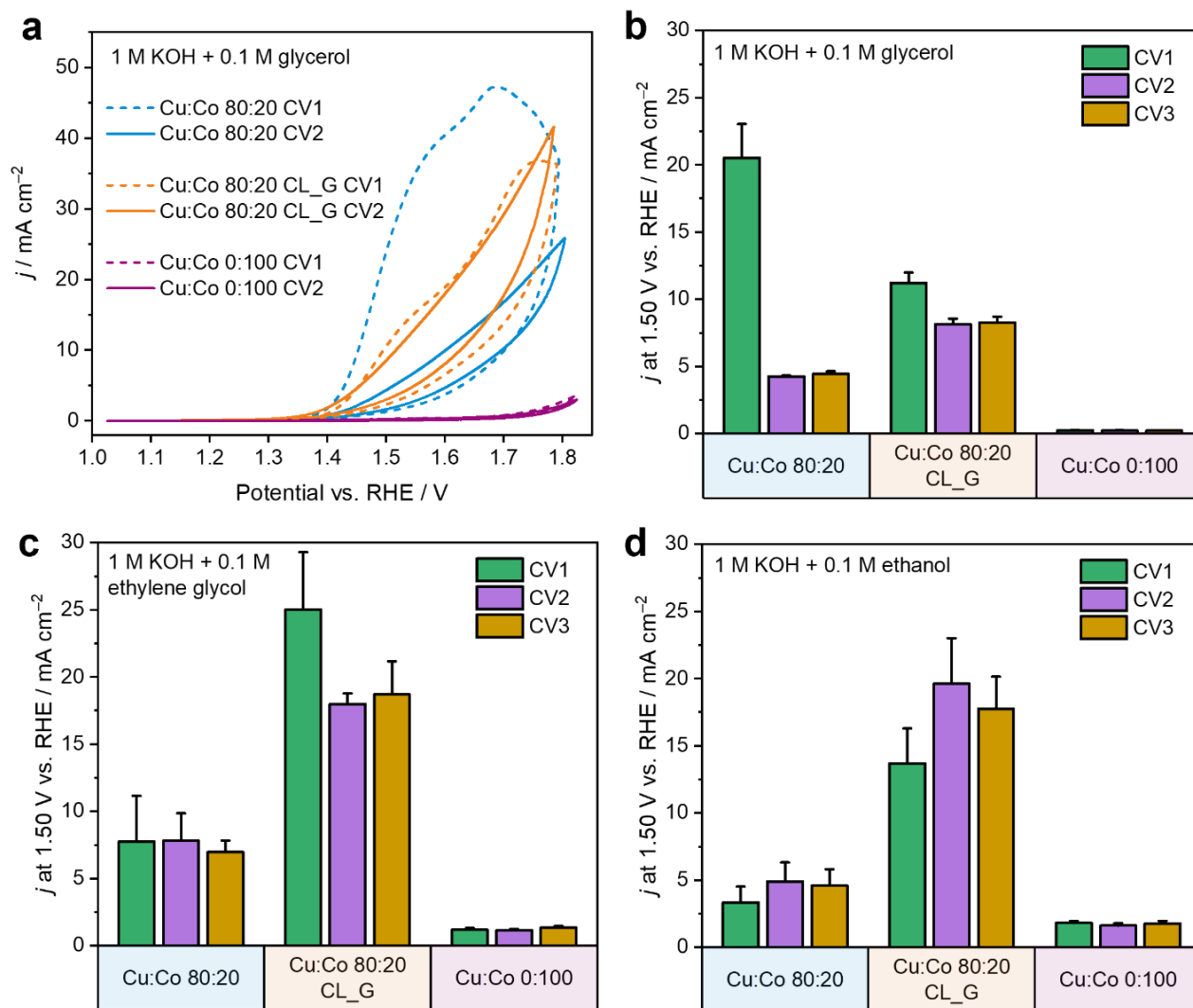
Figure 13. Comparison of the electrocatalytic activity of the chemically leached catalyst, Cu:Co 80:20 CL_G, to the as-prepared Cu:Co 80:20 and the Cu:Co 0:100 catalyst. **a)** First and second CVs recorded in Ar saturated 1 M KOH + 0.1 M glycerol at a scan rate of 5 mV s^{-1} and an electrode rotation of 1600 rpm. **b,c,d)** Current densities recorded in the anodic scan of three consecutive CVs at 1.50 V vs. RHE for the **b)** GOR, **c)** EGOR and **d)** EOR for the corresponding catalyst.

However, apart from the first CV of Cu:Co 80:20 in GOR, we see a general trend for all three types of AOR that the chemically leached sample Cu:Co 80:20 CL_G is the most active compared to the pristine Cu:Co 80:20 and the Cu-free sample Cu:Co 0:100 showing that chemical leaching in glycerol is an interesting pre-treatment step in the preparation of Cu-containing hydroxycar-bonate electrocatalysts that can remove Cu to expose structurally distorted centers that otherwise would not be readily accessible for the electrochemical reaction. Generally, this hypothesis seems to not only hold for the GOR but also for the EGOR and EOR. The use of chemical leaching as an intended preparation step by design to further increase the AOR activity of our co-precipitated hydroxycarbonates will be reported in a forthcoming work.

In an attempt to better discriminate between the two hypothetical contributions to the increased activity, the increase in exposed sites as determined from the surface area, and the effect of structural distortion suggested by the computational results, the recorded currents of Cu:Co 80:20 CL_G during GOR, EGOR and EOR were normalized to the BET surface area and compared to Cu:Co 80:20 and Cu:Co 60:40 which has a similar

Cu:Co ratio and shows a similar kolwezite structure, according to PXRD. The resulting current densities from the anodic scan in the first and third CV were compared at 1.50 V vs. RHE and are shown in Figures S14. In contrast to Figure 13, it can be noticed that Cu:Co 80:20 CL_G is not the most active catalyst compared to the Cu:Co 80:20 catalyst for the AOR anymore indicating that the increased surface area of Cu:Co 80:20 CL_G has an influence on the activity but cannot be considered as the sole factor for the observed increased activity.

For complex reactions such as GOR where highly valuable oxidation products can be obtained, activity and reaction selectivity are essential. Therefore, the GOR selectivity in the presence of different electrocatalysts from the series, including Cu:Co 80:20 CL_G, was investigated in a circular flow cell electrolyzer (Figure 14, Figure S15 to S17) for 4 h and the products were measured each hour at different electrolysis potentials using high-performance liquid chromatography (HPLC). HPLC-chromatograms of the standards and chromatograms obtained on Cu:Co 80:20 CL_G at different potentials are given in Figure S18 and Figure S19 respectively. Irrespective of the used catalyst as well as the reaction time, formate is the major

12

RESEARCH ARTICLE

detectable product with similar faradaic efficiencies (FE) in a range of 50 to 70% at a potential of 1.42 V vs. RHE (Figure 14b and S17) while glycolate is detected with FE < 4% suggesting that the ratio of Cu:Co in the hydroxycarbonate, the local surface structure or the different surface areas do not have a strong influence on the selectivity during GOR.
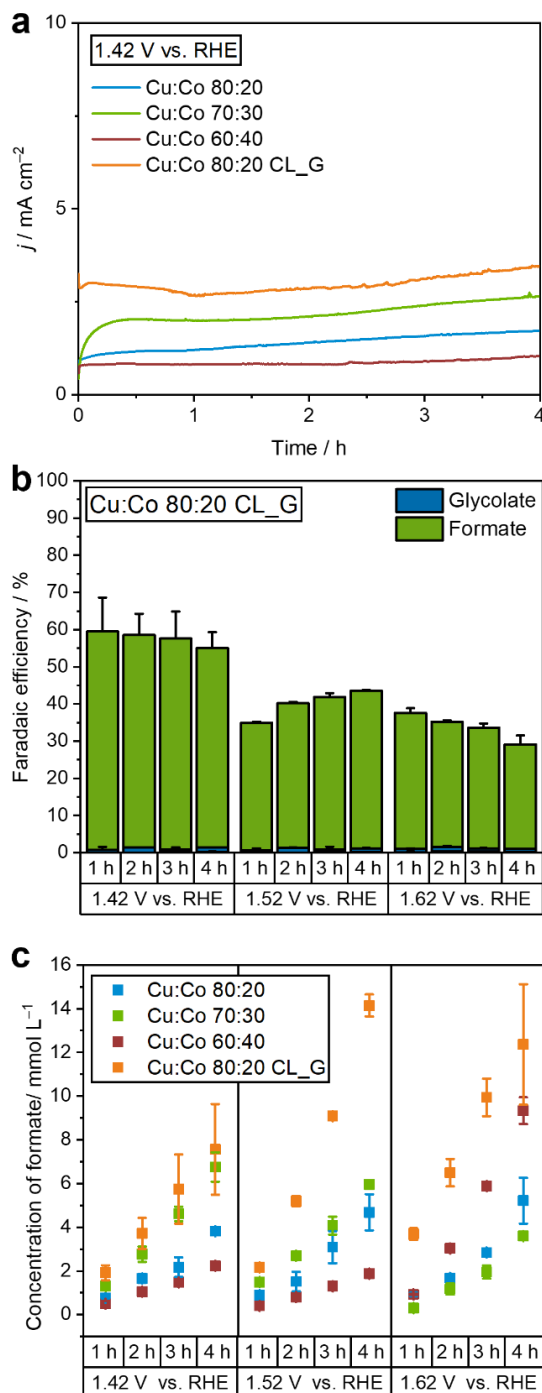

Figure 14. Results from chronoamperometric measurements conducted in circular flow cells using catalysts with a Cu:Co ratio of 80:20, 70:30, 60:40 in comparison to Cu:Co 80:20 CL_G in 1 M KOH and 0.1 M glycerol. **a)** Current density recorded on the tested catalysts at 1.42 V vs. RHE. **b)** Faradaic efficiency of detected GOR products at certain electrolysis times and applied potentials using Cu:Co 80:20 CL_G. **c)** Average concentration of formate measured by HPLC after 1 to 4 h of electrolysis at potentials of 1.42, 1.52 and 1.62 V vs. RHE using selected catalysts.

Interestingly, we see that in the flow cell measurements higher currents are recorded for Cu:Co 80:20 CL_G compared with other catalysts (Figure 14a and Figure S16), which was unexpected considering the RDE results for GOR (Figure S14). Still, it is important to consider that different changes in the reaction environment may occur in a flow cell where we use a much smaller electrolyte volume than in an RDE experiment. For example, formic acid formed during the electrolysis may accumulate during the 4 h electrolysis (Figure 14c) and can be further electrooxidized, leading to an overall increased recorded current. This may partially explain the overall faradaic efficiencies that do not sum-up to 100%, most probably due to further oxidation of the glycerol as well as other intermediates to CO_2 or due to OER, which cannot be detected by HPLC. This becomes more visible, especially for Cu:Co 80:20 CL_G, where a decrease in FE is observed at higher potentials (Figure 14b and Figure S17).

However, despite the detected FEs being similar for all catalysts or even lower at 1.62 V for the Cu:Co 80:20 CL_G, the concentration of formate reaches the highest values on the chemically leached catalyst with 14 mmol L^{-1} at 1.52 V after 4 h of electrolysis. In comparison, just 10 mmol L^{-1} is reached at 1.62 V using Cu:Co 60:40 after 4 h electrolysis (Figure 14c). This represents a clear advantage for using Cu:Co 80:20 CL_G, which allows the highest formate formation rate to be recorded at a lower overpotential than the next best catalyst in the series, Cu:Co 60:40.

Conclusion

A series of hydroxycarbonates with different ratios of Cu and Co were synthesized by co-precipitation followed by a hydrothermal ageing step. Elemental analysis, PXRD and IR measurements showed that the synthesis was successful with certain deviations from the nominal Cu:Co ratios, which led to the identification of three different regions in the composition space: The malachite structure region (Cu:Co ratios of 100:0 to 80:20), the kolwezite structure region (Cu:Co ratios of 70:30 to 50:50) and — with a less pronounced transition — the $Co_2CO_3(OH)_2$ region (Cu:Co ratios of 40:60 to 0:100).

The Cu-Co hydroxycarbonates were investigated as catalysts for the OER, GOR, EGOR and EOR in alkaline solution. It was shown that at higher potentials the OER on the Cu:Co 80:20 catalyst was suppressed in the presence of vicinal alcohols such as glycerol and ethylene glycol, indicating a competition between the different catalytic reactions for the same active sites. Furthermore, different composition-activity correlations depending on the respective oxidation reaction and the number of CV scans were observed using RDE voltammetry. In general, the substitution of Cu by Co led to a boost in activity both in the OER and the AOR. In particular, the Cu:Co 80:20 hydroxycarbonate, for which a medium OER activity among the tested catalysts was obtained, showed the highest initial activity in all alcohol-containing KOH solutions, with the highest GOR activity recorded for Cu:Co 80:20. Further substituting Cu by Co led to a decrease in activity for all the investigated alcohol oxidations, emphasizing the advantage of bimetallic Cu and Co hydroxycarbonates as catalysts for the AOR. The composition-activity correlation in the AOR changed significantly after three CVs, which could partly be attributed to the chemical or electrochemical leaching of Cu in polyalcohol-containing KOH solutions. Additionally, theoretical calculations show that glycerol and glycerolate monoanions coor-

RESEARCH ARTICLE

dinate preferentially on Cu atoms in the Cu-Co hydroxycarbonates and that chemical leaching of Cu from the catalyst that was simulated by changing to a Cu-deficient composition can lead to higher adsorption energies of glycerol/glycerolate on the remaining catalyst, indicating an influence on the electrocatalytic activity. The process of selective chemical leaching was thus deliberately exploited for leaching Cu from the Cu:Co 80:20 catalyst, which yielded a catalyst (Cu:Co 80:20 CL_G) showing higher electrocatalytic activity based on the geometric current densities for the GOR, the EGOR, and the EOR than the pristine Cu:Co 80:20 catalyst and the pure Co hydroxycarbonate. Furthermore, selectivity and stability measurements in a circular flow cell reactor showed an advantage in using Cu:Co 80:20 CL_G for the GOR, as the highest amounts of formate, a value-added product from the GOR, were obtained at low overpotentials compared to other hydroxycarbonates active for the GOR. Selective chemical leaching of Cu has thus emerged as a promising synthetic approach in the preparation of catalysts based on Cu-Co hydroxycarbonates for AOR in alkaline solution.

Experimental Section

Materials and Reagents

Copper nitrate $(Cu(NO_3)_2 \cdot 3 H_2O$ ≥99.5% p.a. ACS, C. Roth), cobalt nitrate $(Co(NO_3)_2 \cdot 6 H_2O$ ≥98% p.a., C. Roth), and sodium carbonate $(Na_2CO_3$ ≥99.5% p.a. ACS, C. Roth) were used without further purification. Glycerol (Fisher Scientific, ≥99%), ethylene glycol (Acros Organics, 99%), ethanol (VWR International, 99.97%), Nafion (Sigma-Aldrich, 5 wt.% in lower aliphatic alcohols and water), Ni foam (Goodfellow), sulfuric acid (Merck, 98%), ammonium formate (Sigma-Aldrich, ≥99%), glycolic acid (Sigma-Aldrich, 99%), calcium L-(–)-glycerate dihydrate (Alfa Aesar) and oxalic acid (Fluorochem) were used as purchased without further purification. KOH solutions (Fisher Scientific, 86.8%) were purified by a Chelex 100 cation-exchange resin (Sigma-Aldrich, 50–100 mesh) to remove metal impurities.[73] All solutions were prepared with ultrapure water.

Synthesis

Hydroxycarbonate precursors were synthesized by co-precipitation ($T = 338$ K) from Cu-Co (1.0 M) nitrate solutions and Na_2CO_3 solution (1.6 M) as a precipitating agent in an automated lab reactor (OptiMax, Mettler Toledo) at constant pH of 8.5. The precipitate was moved to a stainless steel autoclave with a teflon inlet and aged in the mother liquor at hydrothermal conditions (376 K, 20 h), and subsequently filtered, washed (until the conductivity in the wash water was <100 μS cm^{-1}), and dried. (Divergently, the sample Cu100 was not aged in the autoclave, but directly in the lab reactor at precipitation temperature for 30 minutes. Washing and drying were then performed alike.)

Structural Characterisation

X-Ray Powder Diffraction patterns were recorded at room temperature using Cu Kα1,2 radiation on an Empyrean diffractometer (PANalytical) equipped with a 1D PIXcel detector in reflection mode ($2\theta = 10°\cdots80°$, step size 0.05°).

Metal ratios were determined by *Atomic Absorption Spectroscopy* (AAS), performed on a Thermo Fisher iCE-3500 AAS after dissolving the samples in nitric acid overnight. CHNS analysis was carried out by combustion of the sample together with V_2O_5 in a EuroVector EA3000.

ICP-OES Measurements were performed on an Avio 200 ICP Optical Emission Spectrometer equipped with a PerkinElmer S23 Autosampler. For the measurement, 5 mg of a sample were dissolved with trace metal grade nitric acid and then diluted with DI water. For calibration, external calibration standards were created from a Supelco ICP multi-element

standard solution IV from Sigma Aldrich with a concentration of 1000 mg L^{-1} and were diluted with DI water and trace metal grade nitric acid to the final elemental concentrations.

EDX Measurements were performed with a Philips Environmental Scanning Electron Microscope ESEM XL30 equipped with an EDX detector.

Infrared Spectra were recorded at room temperature on a Bruker Vertex 70 FT-IR spectrometer using a broadband spectral range extension (VERTEX FM) for full, mid and far IR in the range of 6.000-80 cm^{-1}.

N_2 Adsorption–Desorption profiles were measured at a BELSORP MAX II sorption station from Mictrotrac with nitrogen 5.0 (99.999 vol.%, Westfalen). The partial pressures referenced to an empty cell were recorded between $p/p_0 = 0.0\cdots0.9$ at 77 K to create the complete isotherm profile. The surface areas of precursors and calcined samples were calculated by applying the Brunauer-Emmett-Teller (BET) equation to the N_2 adsorption data in the range of $p/p_0 = 0.07\cdots0.40$. The sample was first degassed under vacuum at 353 K to remove any adsorbed gases.

Scanning Electron Microscopy was performed with an Apreo S LoVac microscope (Thermo Fisher Scientific) on gold/palladium-sputtered samples.

X-Ray Photoelectron Spectroscopy (XPS) measurements were performed using a VersaProbe II (ULVAC-Phi 5000) with a monochromatic Al Kα source.

Leaching Experiments

Leaching experiments were performed by mixing 400 mg of a sample with 50 mL of a solution consisting of 1 M KOH and 0.1 M of alcohol. The resulting mixture was then stirred at room temperature for 4 h. After leaching, the product was separated from the supernatant by centrifugation and washed with DI water before it was dried in a vacuum oven for 24 h at 333 K.

Electrochemical Characterisation

Electrocatalytic Activity. The electrochemical measurements were performed using a Metrohm Autolab bipotentiostat/galvanostat PGSTAT302N. As electrolyte either 1 M KOH solution or 1 M KOH + 0.1 M alcohol (ethanol, ethylene glycol or glycerol) was used. The electrolyte was purged with Ar for at least 15 min and an Ar flow was maintained close to the electrolyte's surface during the experiment. The RDE experiments were performed using a three-electrode configuration setup. As a working electrode (WE) a glassy carbon electrode (0.113 cm² geometric area) was used, while a platinum coil and a double junction Ag/AgCl (3 M KCl) electrode were used as a counter (CE) and reference electrodes (RE), respectively. The counter electrode was separated by a glass frit from the bulk electrolyte. Catalyst inks of 5 mg mL^{-1} were prepared by dispersing the catalyst powders in a mixture of ultrapure water, ethanol and Nafion solution (volumetric ratio of 49:49:2) and sonicating it for 15 min. 4.78 μL of the ink was drop casted on the polished glassy carbon rotating disk electrode and dried at room temperature for at least 20 min to obtain a catalyst mass loading of 210 μg cm^{-2}. Electrochemical impedance spectra (EIS) were collected at open-circuit potential (OCP) to determine the uncompensated resistance (R_u) in a frequency range of 100 kHz to 1 kHz using a 10 mV (RMS) AC amplitude. Activity measurements were done by cyclic voltammetry in the potential window of 0.0 to 0.8 V vs. Ag/AgCl (3 M KCl) using a scan rate of 5 mV s^{-1} while rotating the WE with a rotation speed of 1600 rpm. Three consecutive cyclic voltammograms were recorded. For each catalyst, all the measurements were conducted in triplicate.

The recorded potentials were converted from the Ag/AgCl (3 M KCl) scale to the reversible hydrogen scale (RHE) using equation 2 and 3.

$$E_{RHE} = E_{measured} + E^0_{Ag/AgCl\,(3\,M\,KCl)} + 0.059\,pH - i \cdot R_u \qquad (2)$$

RESEARCH ARTICLE

$$pH = 14 + \log([OH^-]) + \log(\gamma) \tag{3}$$

E_{RHE} is the working electrode potential with reference to RHE, $E_{measured}$ is the measured potential at the working electrode with reference to Ag/AgCl (3 M KCl), $E^0_{Ag/AgCl\,(3\,M\,KCl)}$ is the formal potential of Ag/AgCl (3 M KCl) vs. RHE, pH denotes the pH value, which was obtained considering the OH⁻ concentration and using an average value of $\gamma = 0.766$[74–76] for the activity coefficient of KOH in water (equation 3), i is the measured current and R_u the uncompensated resistance.

Electrochemical stability – for XPS/SEM measurements. A rectangular-shaped glassy carbon electrode (1x2 cm²) was polished till a mirrorlike surface was obtained. The powder of the catalyst with a Cu:Co ratio of 80:20 was dispersed in a 0.2 vol-% solution of Nafion in ethanol to obtain an ink with a concentration of 5 mg mL⁻¹ after 15 min of sonication. The ink was drop casted on the upper side of the electrode to reach a mass loading of 0.5 mg cm⁻². Afterwards, the electrode was dried in an N_2 stream. The following electrochemical measurement was performed in the same setup used to investigate the electrocatalytic activity. As an electrolyte, 1 M KOH + 0.1 M glycerol was used. The electrolyte was purged with Ar for at least 15 min and an Ar flow was maintained close to the electrolyte's surface during the experiment. The experiment was performed using a three-electrode setup in a 200 mL beaker with the modified glassy carbon electrode as the working electrode. The electrode was immersed in the electrolyte so that 2/3 of the coated part was in contact with the electrolyte, while the third part was not exposed to the electrolyte. Chronoamperometric measurements were carried out at 1.43 V vs. RHE. After 4 h of electrolysis, the electrode was lifted and only 1/3 of the coated electrode was in contact with the electrolyte for another 17 h of electrolysis at 1.43 V vs. RHE. After the electrochemical measurement, the electrode was washed by immersing it several times into ultrapure water and then kept for drying in air overnight.

Electrochemical stability – for PXRD/EDX measurements. Several rectangular-shaped glassy carbon electrodes (1x6 cm²) were prepared similarly as described before, except that the catalyst ink was drop casted on both sides of the electrodes to achieve a mass loading of 0.5 mg cm⁻². The setup for the electrochemical measurements was the same as used before and accordingly, an Ar purged electrolyte, 1 M KOH and 0.1 M glycerol, was utilized. The electrodes were fully submerged in the respective electrolyte and chronoamperometric measurements were performed at 1.43 V vs. RHE for 4 h. After 4 h of electrolysis, the electrodes were dipped several times into ultrapure water and then kept for drying in air overnight. The catalyst was then carefully scratched from the electrode and prepared for analysis.

Determination of electrochemical surface area. The electrochemical surface area (ECSA) of the catalyst with a Cu:Co ratio of 80:20 was evaluated from measuring the electrochemical double-layer capacitance (C_{DL}) in Ar saturated 1 M KOH. Measurements were conducted in a three-electrode RDE setup as described previously. Cyclic voltammograms were recorded in the OCP ± 0.05 V potential window using different scan rates (v): 0.005, 0.01, 0.02, 0.025, 0.03, 0.04, 0.05, 0.08, 0.1, 0.2 and 0.4 V s⁻¹. 10 s waiting time was used between the anodic and the cathodic scans. The double-layer charging current (i_c) was plotted against the scan rate (v) and the electrochemical double-layer capacitance was obtained by fitting to an allometric model using equation 4 as previously described elsewhere.[77] The charging current (i_c) was calculated from the average of the absolute currents from the anodic and the cathodic scan of the respective CV for a given potential in the non-Faradaic region at the respective scan rate.

$$i_c = C_{DL} \cdot v^\alpha \tag{4}$$

The corresponding C_{DL} value was used as an estimation for the ECSA, since a proportional relationship is widely accepted.[78] After the first ECSA determination (0 h) in 1 M KOH, the electrolyte was changed to an Ar-purged solution of 1 M KOH + 0.1 M glycerol. Chronoamperometry at 1.43 V vs. RHE with a rotation speed of 1600 rpm was performed for 2 h. Afterwards, the electrolyte was changed back to 1 M KOH and the

corresponding ECSA measurement was done (2 h). After two more hours of chronoamperometry at 1.43 V vs. RHE (total electrolysis of 4 h), ECSA measurements were repeated similarly. Chronoamperometry was applied for another 17 h (total electrolysis of 21 h) and the last ECSA determination was conducted.

Electrolysis in circular flow cells. Chronoamperometric (CA) measurements were performed in a circular flow cell, containing two compartments, and separated by an anion exchange membrane (Fumatech fumasep FAA-3-PK-130). In the cathode compartment, Ni-foam was used as a counter electrode, while in the anode compartment the catalyst modified carbon paper (H23, Freudenberg, 0.95 cm² geometric area exposed to electrolyte) and an Ag/AgCl (3.4 M KCl) leak-free electrode (Innovative Instruments, Inc.) were used as WE and RE, respectively. The electrolyte was cycled in both compartments by means of a peristaltic pump with a constant flow rate of approximately 7 mL min⁻¹. 1 M KOH solution was introduced in the cathode compartment, while in the anode compartment 0.1 M glycerol and 1 M KOH solution were continuously flowed. Fabrication of the catalyst modified carbon paper used as WE was done by spray coating. The powder catalysts were dispersed in a 0.2 vol.% solution of Nafion in ethanol to generate catalyst inks with a concentration of 1.3 mg mL⁻¹. The spray coating process was performed while heating the carbon support at 125 °C. Multiple layers were sprayed until a close to 0.5 mg cm⁻² mass loading was obtained. Measurements were conducted using Metrohm Autolab bipotentiostat/galvanostat PGSTAT302N or PGSTAT204. Impedance spectra were collected at OCP in a frequency range of 100 kHz to 0.1 kHz using a 10 mV (RMS) AC amplitude and the CA measurements were carried out at 0.4, 0.5 or 0.6 V vs. Ag/AgCl (3.4 M KCl) for 4 h. The obtained current densities and faradaic efficiencies were averaged over two electrodes per potential and catalyst. The applied potentials were converted from the Ag/AgCl (3.4 M KCl) scale to the reversible hydrogen scale (RHE) using equation 2 and 3 and the formal potential of Ag/AgCl (3.4 M KCl).

Product Analysis. 250 µL of the sample was collected manually at different reaction times (1, 2, 3 and 4 h) to investigate the reaction's faradaic efficiency from both anodic and cathodic compartments. The samples were diluted with 300 µL of 0.5 M H_2SO_4 directly after sampling and before performing HPLC measurements to avoid the chemical transformation of unstable intermediates. Measurements were conducted on the AZURA HPLC system (Knauer) with a refractive index detector (RID 2.1L, Knauer) and a diode array detector (UV/VIS, DAD 2.1L, Knauer). An ion exclusion column (Eurokat H, Knauer) and the respective precolumn were used at 70 °C and a flow rate of 0.6 mL min⁻¹ with 5 mM H_2SO_4 as the eluent to separate the products obtained from GOR. Products were assigned by calibration with commercially available reference compounds. The products were measured by an RI detector (RID). The UV/VIS detector at 220 nm was used to detect formic acid because glycerol and formic acid overlap in RI. Glycerol concentrations were calculated by subtracting the peak area of formic acid in the RI scale, whose concentration was determined before at 220 nm, from the whole peak area of glycerol and formic acid in the RID using the respective calibration factors. Concentrations were converted to moles by using the anolyte and catholyte volumes corrected by the sampled volume. The faradaic efficiency was calculated by equation 5.[39]

$$\text{Faradaic efficiency} = \frac{1}{v_P} \cdot \frac{(n_{t,product} - n_{i,product}) \cdot F \cdot n(e^-)}{Q_{total}} \cdot 100\% \tag{5}$$

v_P	Stoichiometric factor,
$n_{t,product}$	Number of moles of the respective product at time t in mol,
$n_{i,product}$	Initial number of moles of the respective product in mol,
F	Faraday's constant; 96485 C mol⁻¹,
$n(e^-)$	Number of electrons from the oxidation of 1 mol of glycerol into the respective product in mol,
Q_{total}	Total charge passed WE during electrolysis in C.

Differential Electrochemical Mass Spectrometry (DEMS) was used for in-situ detection of oxygen during cyclic voltammetry. Mass spectra were

Electrochemistry during DEMS experiments was performed on a Biologic VSP-300 potentiostat. Cyclic voltammetry was recorded from +1 to +1.8 V vs. RHE at a scan rate of 0.5 mV s^{-1}. A 5 Hz filter was used to eliminate noise from potential measurement as a result of the electrolyte flow. The electrolyte was circulated through the cell in a continuous flow mode with a rate of 10 µL min^{-1} by means of a syringe pump. The DEMS electrochemical cell was a single-compartment thin-layer cell made of PEEK with a three-electrode configuration (supplied by HIDEN Analytical Ltd.). The working electrode was a glassy carbon rod of 5 mm of diameter with the catalyst drop-coated on top, with a loading of 0.2 mg cm^{-2}. The counter electrode was a Pt wire of 0.5 mm of diameter set at the outlet of the electrolyte and the reference electrode was a leakless Ag/AgCl (3.4 M KCl) reference electrode (Innovative Instruments, Inc., USA). A 28 µm-thickness PTFE membrane with a pore size of 20 nm was located between the thin-layer cell and the mass spectrometer inlet port. DEMS signals were processed to minimize the influence of bubbles noise on the recorded trends. The processing was performed by the smoothing method LOWESS (proportion for Span, Span 0.1) of the software "Origin Pro 2020". Also, DEMS signals shown are background subtracted.

In order to estimate the faradaic currents of OER from DEMS signals, the relationship between the m/z 32 DEMS signals and the corresponding O_2 faradaic currents was investigated by a proper calibration. The calibration was conducted with a reported active and stable OER catalyst, a Co-hydroxynitrate[79], in an alcohol-free 1 M KOH solution. This catalyst provided 100% of OER faradaic efficiency in 1 M KOH at least up to 50 mA cm^{-2}. The calibration was made with the same conditions as the measurements, including the electrocatalyst film preparation. After that, the expression in equation 6 was found and used to convert the obtained DEMS signals in the respective faradaic currents (Figure S20).

O_2 faradaic current (mA) = m/z 32 DEMS signal (nTorr) · 5.319 mA nTorr^{-1}

(6)

Calculations

Structures of mixed Cu-Co hydroxycarbonate clusters with Cu:Co ratio 80:20 and pure Cu and Co hydroxycarbonate clusters of the general composition $(Cu,Co)_2CO_3(OH)_2 \times 5$ were globally optimized at the semiempirical GFN2-xTB level[80,81], employing evolutionary algorithms as implemented in the OGOLEM program framework.[82–84] For each composition, 3 runs were carried out with 70,000 steps each for the mixed clusters and 50,000 steps for the pure clusters, due to the larger search space of the former. The cluster pool was initialized with 40 random cluster structures. In every step, two individuals were selected based on a Gaussian distribution over the minimal total energy, with Gaussian widths 0.2 and 0.01, respectively, providing a mix of exploration towards new structures and exploitation by small improvements of best-so-far clusters. During the phenotype crossover operation, the selected clusters were cut once or twice by randomly positioned and oriented planes. One part of each was then swapped into the other. This was followed by a mutation operation where one or more atoms were moved using Monte Carlo methods. From the resulting two new structures, the one with the lower total energy was chosen and inserted back into the pool, obeying both an energy-based diversity limit and a structure-based niching employing the Coulomb matrix.[85] Prior to the local optimization with the above-mentioned GFN2-xTB method, short-distance atom pairs were shifted slightly apart by our "detangler" preprocessor,[86] employing a simple, repulsive Gaussian shaped, artificial pair potential, to avoid convergence problems during the ensuing local optimization. Via the standard interface between OGOLEM and the external xTB code, local optimization at the GFN2-xTB level was then carried out within the latter program package, with the default convergence criterion for the optimization and assuming 10 unpaired electrons.

Possible glycerol adsorption sites and configurations were scanned by systematically placing one single glycerol molecule (as such, or deprotonated) in four different start positions on a regular, evenly distributed, spherical grid of 300 points around the above-mentioned clusters, followed by an overall local structure minimization. For the resulting adsorbed structures, adsorption energies were determined at the same level of theory, as the total energy difference between the adsorbed state and the dissociated state, with internal relaxation of the latter, i. e.,

adsorption energy = E(cluster,glycerol) − E(cluster) − E(glycerol).

[1]   N. Armaroli, V. Balzani, *ChemSusChem* **2011**, *4*, 21–36.
[2]   J. A. Turner, *Science* **2004**, *305*, 972–974.
[3]   J. Song, C. Wei, Z.-F. Huang, C. Liu, L. Zeng, X. Wang, Z. J. Xu, *Chem. Soc. Rev.* **2020**, *49*, 2196–2214.
[4]   B. Garlyyev, S. Xue, J. Fichtner, A. S. Bandarenka, C. Andronescu, *ChemSusChem* **2020**, *13*, 2513–2521.
[5]   L. Chen, J. Shi, *J. Mater. Chem. A* **2018**, *6*, 13538–13548.
[6]   F. Arshad, T. u. Haq, I. Hussain, F. Sher, *ACS Appl. Energy Mater.* **2021**, *4*, 8685–8701.
[7]   Y. Xu, B. Zhang, *ChemElectroChem* **2019**, *6*, 3214–3226.
[8]   B. You, Y. Sun, *Acc. Chem. Res.* **2018**, *51*, 1571–1580.
[9]   Y. Li, X. Wei, L. Chen, J. Shi, M. He, *Nat. Commun.* **2019**, *10*, 5335.
[10]   X. Wang, S. Xi, W. S. V. Lee, P. Huang, P. Cui, L. Zhao, W. Hao, X. Zhao, Z. Wang, H. Wu, H. Wang, C. Diao, A. Borgna, Y. Du, Z. G. Yu, S. Pennycook, J. Xue, *Nat. Commun.* **2020**, *11*, 4647.
[11]   Y. Huang, X. Chong, C. Liu, Y. Liang, B. Zhang, *Angew Chem.* **2018**, *130*, 13347–13350.
[12]   L. Sha, J. Yin, K. Ye, G. Wang, K. Zhu, K. Cheng, J. Yan, G. Wang, D. Cao, *J. Mater. Chem. A* **2019**, *7*, 9078–9085.
[13]   X. Ma, J. Wang, D. Liu, R. Kong, S. Hao, G. Du, A. M. Asiri, X. Sun, *New J. Chem.* **2017**, *41*, 4754–4757.
[14]   W. Huang, X.-Y. Ma, H. Wang, R. Feng, J. Zhou, P. N. Duchesne, P. Zhang, F. Chen, N. Han, F. Zhao, J. Zhou, W.-B. Cai, Y. Li, *Adv. Mater.* **2017**, *29*, 1703057.
[15]   D. Martín-Yerga, G. Henriksson, A. Cornell, *Electrocatalysis* **2019**, *10*, 489–498.
[16]   Q. Lin, Y. Wei, W. Liu, Y. Yu, J. Hu, *Int. J. Hydrog. Energy* **2017**, *42*, 1403–1411.
[17]   B. Yan, H. Xu, K. Zhang, S. Li, J. Wang, Y. Shi, Y. Du, *Appl. Surf. Sci.* **2018**, *434*, 701–710.
[18]   Y. Kwon, K. J. P. Schouten, M. T. M. Koper, *ChemCatChem* **2011**, *3*, 1176–1185.
[19]   M. S. E. Houache, K. Hughes, R. Safari, G. A. Botton, E. A. Baranova, *ACS Appl. Mater. Interfaces* **2020**, *12*, 15095–15107.
[20]   A. C. Brix, D. M. Morales, M. Braun, D. Jambrec, J. R. C. Junqueira, S. Cychy, S. Seisel, J. Masa, M. Muhler, C. Andronescu, W. Schuhmann, *ChemElectroChem* **2021**, *8*, 2336–2342.

[21] J. C. Beltrán-Prieto, K. Kolomazník, J. Pecha, *Aust. J. Chem.* **2013**, *66*, 511.

[22] R. Ciriminna, C. Della Pina, M. Rossi, M. Pagliaro, *Eur. J. Lipid Sci. Technol.* **2014**, *116*, 1432–1439.

[23] J. A. Kenar, *Lipid Technol.* **2007**, *19*, 249–253.

[24] L. Fan, B. Liu, X. Liu, N. Senthilkumar, G. Wang, Z. Wen, *Energy Technol.* **2020**, 2000804.

[25] P. A. Alaba, C. S. Lee, F. Abnisa, M. K. Aroua, P. Cognet, Y. Pérès, W. M. A. Wan Daud, *Rev. Chem. Eng.* **2020**, *0*, 116.

[26] D. M. Morales, D. Jambrec, M. A. Kazakova, M. Braun, N. Sikdar, A. Koul, A. C. Brix, S. Seisel, C. Andronescu, W. Schuhmann, *ACS Catal.* **2022**, *12*, 982–992.

[27] B. You, X. Liu, X. Liu, Y. Sun, *ACS Catal.* **2017**, *7*, 4564–4570.

[28] S. Barwe, J. Weidner, S. Cychy, D. M. Morales, S. Dieckhöfer, D. Hiltrop, J. Masa, M. Muhler, W. Schuhmann, *Angew. Chem. Int. Ed.* **2018**, *57*, 11460–11464.

[29] Z. Miao, C. Xu, J. Zhan, Z. Xu, *J. Alloys Compd.* **2021**, *855*, 157438.

[30] A. El Attar, L. Oularbi, S. Chemchoub, M. El Rhazi, *Int. J. Hydrog. Energy* **2020**, *45*, 8887–8898.

[31] L. Dai, Q. Qin, X. Zhao, C. Xu, C. Hu, S. Mo, Y. O. Wang, S. Lin, Z. Tang, N. Zheng, *ACS Cent. Sci.* **2016**, *2*, 538–544.

[32] M. A. Abdelkareem, E. T. Sayed, H. Alawadhi, A. H. Alami, *Int. J. Hydrog. Energy* **2020**, *45*, 17311–17319.

[33] C. Chen, S. Zhu, X. Yang, L. Pi, Z. Cui, *Electrochim. Acta* **2011**, *56*, 10253–10258.

[34] S. Sun, L. Sun, S. Xi, Y. Du, M. U. Anu Prathap, Z. Wang, Q. Zhang, A. Fisher, Z. J. Xu, *Electrochim. Acta* **2017**, *228*, 183–194.

[35] P. V. Santiago, C. C. Lima, J. L. Bott-Neto, P. S. Fernández, C. A. Angelucci, J. Souza-Garcia, *J. Electroanal. Chem.* **2021**, *896*, 115198.

[36] T.-G. Vo, P.-Y. Ho, C.-Y. Chiang, *Appl. Catal. B* **2022**, *300*, 120723.

[37] C. Liu, M. Hirohara, T. Maekawa, R. Chang, T. Hayashi, C.-Y. Chiang, *Appl. Catal. B* **2020**, *265*, 118543.

[38] S. Zhu, A. Xie, X. Tao, J. Zhang, B. Wei, Z. Liu, Y. Tao, S. Luo, *J. Electroanal. Chem.* **2020**, *857*, 113748.

[39] X. Han, H. Sheng, C. Yu, T. W. Walker, G. W. Huber, J. Qiu, S. Jin, *ACS Catal.* **2020**, 6741–6752.

[40] G. A. El-Nagar, I. Derr, T. Kottakkat, C. Roth, *ECS Trans.* **2017**, *80*, 1013–1022.

[41] K. Chakrapani, F. Özcan, K. F. Ortega, T. Machowski, M. Behrens, *ChemElectroChem* **2018**, *5*, 93–100.

[42] F. Yang, K. Sliozberg, I. Sinev, H. Antoni, A. Bähr, K. Ollegott, W. Xia, J. Masa, W. Grünert, B. R. Cuenya, W. Schuhmann, M. Muhler, *ChemSusChem* **2017**, *10*, 156–165.

[43] J. Jiang, A. Zhang, L. Li, L. Ai, *J. Power Sources* **2015**, *278*, 445–451.

[44] Z. Li, M. Shao, H. An, Z. Wang, S. Xu, M. Wei, D. G. Evans, X. Duan, *Chem. Sci.* **2015**, *6*, 6624–6631.

[45] F. Song, X. Hu, *J. Am. Chem. Soc.* **2014**, *136*, 16481–16484.

[46] M. Behrens, R. Schlögl, *Z. anorg. allg. Chem.* **2013**, *639*, 2683–2695.

[47] D. Waller, D. Stirling, F. S. Stone, *Faraday Discuss. Chem. Soc.* **1989**, 107–120.

[48] A. Karmakar, S. K. Srivastava, *ACS Appl. Energy Mater.* **2020**, *3*, 7335–7344.

[49] J. Li, X. Li, Y. Luo, Q. Cen, Q. Ye, X. Xu, F. Wang, *Int. J. Hydrog. Energy* **2018**, *43*, 9635–9643.

[50] Y. Wang, W. Ding, S. Chen, Y. Nie, K. Xiong, Z. Wei, *Chem. Commun.* **2014**, *50*, 15529–15532.

[51] K. Karthick, S. Subhashini, R. Kumar, S. Sethuram Markandaraj, M. M. Teepikha, S. Kundu, *Inorg. Chem.* **2020**, *59*, 16690–16702.

[52] T. Tang, W.-J. Jiang, S. Niu, N. Liu, H. Luo, Y.-Y. Chen, S.-F. Jin, F. Gao, L.-J. Wan, J.-S. Hu, *J. Am. Chem. Soc.* **2017**, *139*, 8320–8328.

[53] S. Zhang, B. Ni, H. Li, H. Lin, H. Zhu, H. Wang, X. Wang, *Chem. Commun.* **2017**, *53*, 8010–8013.

[54] J. Schumann, T. Lunkenbein, A. Tarasov, N. Thomas, R. Schlögl, M. Behrens, *ChemCatChem* **2014**, *6*, 2889–2897.

[55] M. Deliens, P. Piret, *Bull. Soc. Fr. Mineral. Cristallogr.* **1980**, *103*, 179–184.

[56] N. Perchiazzi, R. Dragone, N. Demitri, P. Vignola, C. Biagioni, *Eur. J. Mineral.* **2018**, *30*, 609–620.

[57] J. González-López, J. K. Cockcroft, Á. Fernández-González, A. Jimenez, R. Grau-Crespo, *Acta Cryst.* **2017**, *B73*, 868–873.

[58] N. Perchiazzi, *Z. Kristallogr. Suppl.* **2006**, *23*, 505–510.

[59] F. Girgsdies, S. Tolborg, M. Behrens, *unpublished*.

[60] B. Lafuente, R. T. Downs, H. Yang, N. Stone, (Eds: T. Armbruster; R. M. Danisi), *Highlights in mineralogical crystallography*, W. De Gruyter, **2015**, Ch. 1.

[61] Y. Kwon, S. C. S. Lai, P. Rodriguez, M. T. M. Koper, *J. Am. Chem. Soc.* **2011**, *133*, 6914–6917.

[62] R. M. Sandrini, J. R. Sempionatto, E. Herrero, J. M. Feliu, J. Souza-Garcia, C. A. Angelucci, *Electrochem. commun.* **2018**, *86*, 149–152.

[63] G. B. Kauffman, M. Karbassi, *J. Chem. Educ.* **1985**, *62*, 878.

[64] P. Sivasakthi, R. Sekar, G. N. K. Ramesh Bapu, *Trans. Inst. Met. Finish.* **2015**, *93*, 32–37.

[65] K. F. Gadd, *Educ. Chem.* **1981**, *18*, 176–178.

[66] E. Norkus, A. Vaskelis, J. Vaitkus, J. Reklaitis, *J. Inorg. Biochem.* **1995**, *60*, 299–302.

[67] S. Brunauer, P. H. Emmett, E. Teller, *J. Am. Chem. Soc.* **1938**, *60*, 309–319.

[68] C. Busó-Rogero, E. Herrero, J. M. Feliu, *ChemPhysChem* **2014**, *15*, 2019-2028.

[69] R. Teles, A. Arenillas, G. da Silva, P. S. Fernández, E. S. F. Cardoso, G. Maia, C. A. Martins, *Electrocatalysis* **2017**, *8*, 151-163.

[70] R. S. Ferreira Jr., M. J. Giz, G. A. Camara, *J. Electroanal. Chem.* **2013**, *697*, 15-20.

[71] M. C. Biesinger, B. P. Payne, A. P. Grosvenor, L. W. Lau, A. R. Gerson, R. S. Smart, *Appl. Surf. Sci.* **2011**, *257*, 2717–2730.

[72] D. A. Skoog, D. M. West, F. J. Holler, S. R. Crouch, *Fundamentals of analytical chemistry*, Cengage, Boston, USA, **2021**, Ch. 7.

[73] A. S. Hall, Y. Yoon, A. Wuttig, Y. Surendranath, *J. Am. Chem. Soc.* **2015**, *137*, 14834-14837.

[74] M. Knobel, *J. Am. Chem. Soc.* **1923**, *45*, 70–76.

[75] W. J. Hamer, Y.-C. Wu, *J. Phys. Chem. Ref. Data* **1972**, *1*, 1047–1100.

[76] L. A. Bromley, *AIChE J.* **1973**, *19*, 313–320.

[77] D. M. Morales, M. Risch, *J. Phys. Energy* **2021**, *3*, 34013.

[78] C. C. L. McCrory, S. Jung, J. C. Peters, T. F. Jaramillo, *J. Am. Chem. Soc.* **2013**, *135*, 16977–16987.

[79] A. V. Radha, S. Weiß, I. Sanjuán, M. Ertl, C. Andronescu, J. Breu, *Chem. Eur. J.* **2021**, *27*, 16930–16937.

[80] C. Bannwarth, S. Ehlert, S. Grimme, *J. Chem. Theory Comput.* **2019**, *15*, 1652–1671.

[81] C. Bannwarth, E. Caldeweyher, S. Ehlert, A. Hansen, P. Pracht, J. Seibert, S. Spicher, S. Grimme, *WIREs Comput. Mol. Sci.* **2021**, *11*, e01493.

[82] J. M. Dieterich, B. Hartke, *Mol. Phys.* **2010**, *108*, 279–291.

[83] B. Hartke, *WIREs Comput. Mol. Sci.* **2011**, *1*, 879–887.

[84] C. Witt, M.-C. Schmidt, C. Schröder, S. Schauermann, B. Hartke, *J. Phys. Chem. C* **2021**, *125*, 26167–26179.

[85] M. Dittner, B. Hartke, *Comput. Theor. Chem.* **2017**, *1107*, 7–13.

[86] D. Behrens, *Dissertation*, Christian-Albrecht University, Kiel, **2023**.

WILEY-VCH

RESEARCH ARTICLE

Entry for the Table of Contents
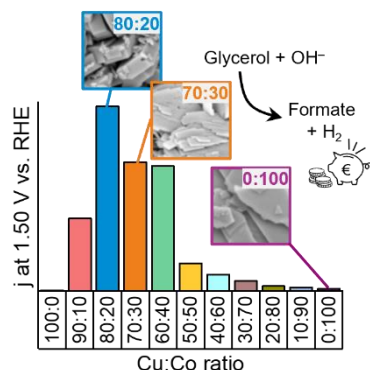
Replacing the oxygen evolution reaction at the anode by the oxidation of alcohols such as glycerol to value-added products can make green hydrogen production by electrochemical water splitting economically feasible. For the first time, a series of low-cost 3d transition metal-based mixed Cu and Co hydroxycarbonates was prepared and investigated as electrocatalysts for the oxidation of glycerol, ethylene glycol and ethanol.

Institute and/or researcher Twitter usernames:

Corina Andronescu @AndronescuLab
Dulce M. Morales @DulesMMH

Additional Author information for the electronic version of the article.

	ORCiD identifier
M. Braun:	0000-0002-3961-6211
G. Behrendt:	0000-0003-3730-967X
M. L. Krebs:	0000-0002-0908-4816
P. Dimitri:	/
P. Kumar:	0000-0002-8088-4672
I. Sanjuán:	0000-0002-5883-7095
S. Cychy:	0000-0002-3264-6282
A. C. Brix:	0000-0002-5660-989X
D. M. Morales:	0000-0002-9420-2724
J. Hörlöck:	/
B. Hartke:	0000-0001-8480-0862
M. Muhler:	0000-0001-5343-6922
W. Schuhmann:	0000-0003-2916-5223
M. Behrens:	0000-0003-3407-5011
C. Andronescu:	0000-0002-1227-1209